UPPSALA
UNIVERSITET

Digital Comprehensive Summaries of Uppsala Dissertations from the Faculty of Science and Technology 875

Molecular Electronics

Insight from Ab-Initio Transport Simulations

JARIYANEE PRASONGKIT

ACTA
UNIVERSITATIS
UPSALIENSIS
UPPSALA
2011

ISSN 1651-6214
ISBN 978-91-554-8208-4
urn:nbn:se:uu:diva-160474

Dissertation presented at Uppsala University to be publicly examined in Å80101, Ångströmlaboratoriet, Lägerhyddsvägen 1, Uppsala. Thursday, December 8, 2011 at 10:15 for the degree of Doctor of Philosophy. The examination will be conducted in English.

Abstract
Prasongkit, J. 2011. Molecular Electronics: Insight from Ab-Initio Transport Simulations. Acta Universitatis Upsaliensis. *Digital Comprehensive Summaries of Uppsala Dissertations from the Faculty of Science and Technology* 875. 67 pp. Uppsala. ISBN 978-91-554-8208-4.

This thesis presents the theoretical studies of electronic transport in molecular electronic devices. Such devices have been proposed and investigated as a promising new approach that complements conventional silicon-based electronics. To design and fabricate future nanoelectronic devices, it is essential to understand the conduction mechanism at a molecular or atomic level. Our approach is based on the non-equilibrium Green's function method (NEGF) combined with density functional theory (DFT). We apply the method to study the electronic transport properties of two-probe systems consisting of molecules or atomic wires sandwiched between leads. A few molecular electronic devices are characterized; namely, conducting molecular wires, molecular switches and molecular recognition sensors. The considered applications are interconnection of different nanoelectronic units with cumulene molecular wires; adding switching functionality to the molecular connectors by applying stress to the CNT-cumulene-CNT junction or by introducing phthalocyanine unit; sensing of individual nucleotides, e.g., for DNA sequencing applications. The obtained results provide useful insights into the electron transport properties of molecules. Several interesting and significant features are analyzed and explained in particular such as, level pinning, negative differential resistance, interfering of conducting channels etc.

Keywords: Molecular Electronics, Ab Initio, DNA Sequencing, Nanoscience, Graphene

Jariyanee Prasongkit, Uppsala University, Department of Physics and Astronomy, Materials Theory, Box 516, SE-751 20 Uppsala, Sweden.

ISSN 1651-6214
ISBN 978-91-554-8208-4
urn:nbn:se:uu:diva-160474 (http://urn.kb.se/resolve?urn=urn:nbn:se:uu:diva-160474)

To My Family

List of Papers

This thesis is based on the following papers, which are referred to in the text by their Roman numerals.

I **Cumulene molecular wire conductance from first principles**
J. Prasongkit, A. Grigoriev, G. Wendin and R. Ahuja, *Phys. Rev. B* **81**, 115404 (2010).

II **Conductance of linear carbon wires bridging carbon nanotubes**
J. Prasongkit, A. Grigoriev, and R. Ahuja, *In manuscript*

III **Interference effects in phtalocyanine controlled by H-H tautomerization: potential two-terminal unimolecular electronic switch**
J. Prasongkit, A. Grigoriev, G. Wendin and R. Ahuja, *Phys. Rev. B* **84**, 165437 (2011).

IV **Transverse conductance of DNA nucleotides in a graphene nanogap from first principles**
J. Prasongkit, A. Grigoriev, B. Pathak, R. Ahuja, and R. H. Scheicher, *Nano Lett.* **81**, 1941 (2011).

V **Transverse electronic transport through DNA nucleotides with functionalized graphene electrodes**
J. Prasongkit, A. Grigoriev, B. Pathak, R. Ahuja, and R. H. Scheicher, *Submitted*.

The following paper is co-authored by me but is not included in this thesis.

• **Crystal structure of the pressure-induced metallic phase of SiH4 from ab initio theory**

D. Y. Kim, R. H. Scheicher, S. Lebégue, J. Prasongkit, B. Arnaud, M. Alouani and R. Ahuja, *PNAS* **105**, 16454 (2008).

• **Double functionalized nanopore embedded gold electrodes for rapid DNA sequencing**

B. Pathak, H. Löfas, J. Prasongkit, A. Grigoriev, R. H. Scheicher and R. Ahuja, *Submitted*

• **Extensive tuning of charge transport through saturated molecular segments revealing the potential of hyperconjugation in molecular junctions**

R. Emanuelsson, J. Prasongkit, A. Grigoriev, R. Ahuja and H. Ottosson, *In manuscript*

Table 1: *My contribution to the papers is indicated.*

Paper	Designing research	Performing calculations	Analyzing data	Coordinating project	Writing the paper
I	•	•	•	•	•
II	•	•	•	•	•
III	•	•	•	•	•
IV	•	•	•	•	•
V	•	•	•	•	•

Contents

1. Introduction

1.1 Electron transport in nanoscale devices

During the last decades, rapid development of electronics has produced the new and fast devices at nanoscale dimensions. This development has continued to follow Moore's Law [1], which states that transistor density on integrated circuits doubles every two years. Nowadays, the heart of modern integrated electronic circuits is based on CMOS (complementary metal-oxide-semiconductor) technology, used in microprocessors, microcontrollers, and other digital logic circuits. CMOS has now scaled down into the nanoscale regime with 65 nm line width [2], while the transistor gate length is even smaller with the order of 35 nm. In 2009, Intel has successfully produced shipments of microprocessors based on 32 nm logic technology [3]. To continue down-scaling these devices, fundamental difficulties will be faced; for instance, the gate leakage current via direct tunneling through the oxide, leading to power dissipation and excessive heat [4]. In addition, the lithographic process is more difficult to control and would probably not be considered for high volume manufacturing [5]. Since the difficulties in miniaturization CMOS technology based on silicon, there has been significant attention to seek alternative technologies, which can outperform the CMOS technology.

One promising idea is constructing the integrated circuit at an atomic or molecular level. In December 1959, at the annual meeting of the American Physical Society, Richard Feynman has introduced the idea of nanoelectronics during his famous speech "Plenty of Room at the Bottom". However, a picture of current flowing through nanoscale devices has brought up many questions. How does the electron flow through nanoscale conductors? Can we use Ohm's law to explain the electron transport in nanoscale devices? A number of studies have been performed showing that Ohm's law fails [6–8]; for example, resistance of quantum wire does not depend on its length since the electron transport is not a diffusion process as described by this simple law. To describe such a small device, one needs a quantum-mechanic treatment of the electrons, in which the quantum effects, such as the discreteness of charge, the energy quantization, and the quantum coherence are to be considered.

Over the past two or three decades, there has been substantial progress both in experimental techniques and in the quantum transport theory that allow us to understand basic properties at the molecular scale and explore the potential use as a basic building block for next generation nanoelectronic devices.

This field is known as molecular electronics, which will be introduced in the following section.

1.2 Molecular electronics

Molecular electronics, one of the major fields of current development in nanoscience. Development of the electronic devices at the molecular scale involves study of the electronic level structure, response and charge transport at atomic scale [9]. These devices can be constructed of single molecules, small groups of molecules, carbon nanotubes, nanoscale metallic or semiconductor wires. Molecular electronics emerging applications are tremendously exciting; for example, molecules can function as transistors [10–12], switches [13–15], rectifiers [16, 17], interconnects [18, 19], photovoltaics [22], memories [23, 24], and sensors [25, 26].

From a point of view of potential technology, molecular electronics is based on a bottom-up approach, piecing together an elementary unit such as molecules to build up electronic circuits. The current flow at the smallest possible unit can be studied by assembling single molecules or small molecular ensembles in between nanometer-scale contacts. In contrast, a top-down approach, miniaturizing macroscopic systems of conventional silicon-based electronics, uses methods such as cutting, moulding or etching and lithography process [27].

Today, molecular electronics is still a rather young field, and unlikely to replace the silicon-based electronics. However, in a long-term goal, we can certainly take an advantage of the properies of the molecular devices that are difficult to implement in the conventional electronics.

Using molecules as electronic components has several potential advantages [28]:

(i) The size of molecules is in the length scale of approximately 1-10 nanometer range.

(ii) The molecular recognition can be employed in changing electronic properties of molecules, which can provide sensing or switching capabilities.

(iii) With their variability of compositions and geometries, one can tune the transport properties of molecules through chemical synthesis.

(iv) A large number of identical molecules can be cheaply produced.

However, molecules have obvious disadvantages:

(i) The stability and the robustness at elevated temperature limits the reliability of many applications.

(ii) It is hard to control the connection between the molecule and the electrodes due to very small size of the structures.

(iii) It is difficult to interface the molecular device with other components in a system that is not a nanoscopic scale.

The first suggestion of molecular electronics was put forward by Ratner and Aviram [29] in 1974. They proposed a molecular structure that could function as electronic component. Such a molecule consists of electron donor and acceptor groups, separated by a molecular bridge. They envisioned the charge transfer as three steps; the electron flow from the cathode to the acceptor unit, then from the acceptor to the donor unit inside the molecule, and finally from the donor unit to the anode. When the molecules were connected to electrodes at finite bias, an asymmetric current-voltage characteristic curve would be observed. These molecules were called as the molecular rectifier, which was the first proposal to use a single molecule as an electronic component. However, Aviram-Ratner's idea did not have a significant impact at that time since there was no real experiment to approve it.

During the early 1990s, molecular electronics has been rapidly developed due to advancements in the experiment techniques. A large number of molecules were discovered, providing the functionalities for electronic components. In parallel, theoretical models have been developed to investigate the conduction mechanism at a molecular scale. In the next section, we will provide a brief introduction to some experimental techniques and theoretical approach related in this thesis.

1.3 Device and theoretical prospects

The first conductance measurement down to single-molecular level was introduced by Reed et al. [30]. They used a mechanically controllable break junction (MCBJ) technique to measure the electrical transport properties of benzenedithiol molecules bridging between two gold electrodes. The MCBJ technique provides a reliable conductance measurement by precisely controlling the distance between two metal electrodes to match with the length of a single molecule [31]. This technique has been now developed for various experimental conditions, for example, in a liquid solution [32], in vacuum [33] and under ambient conditions [34]. Although it offers the robust mechanical stability, but one cannot control the breaking process, the local geometry and configuration of the point contact.

A way to visualize and accurately manipulate matter at an atomic scale is using a scanning tunneling microscope (STM), introduced in 1981. After the invention, the STM was has been used for the fabrication of atomic-size contacts and study the electronic transport properties. The great advantages of this technique are that the single atom and molecules on the surface can be imaged, and current-voltage can be repeatedly measured for several different molecules [35]. However, the crucial drawback of the STM is its poor stability under the change of conditions such as the temperature or magnetic fields. In addition, the vacuum gap between the STM tip and the molecules provides an additional tunneling barrier.

At present, new experimental techniques has been used to address and investigate single or a few molecules, for example, electromigration methods [36] or electro-deposition [37, 38], nanopore [39] and nanogap [40] techniques. Moreover, several attempts have been made to implement a third electrode, used for tuning the conductance of the molecule [41, 42].

The advent of experimental progress in molecular electronics has given rise new challenges to theory in developing theoretical tools to describe the electron transport in molecular devices. The density functional theory (DFT) is now a well-established method for electronic structure calculations of the ground-state properties of metals, semiconductors and insulators [43]. The DFT has become the most popular computational tools for studying bulk materials, molecules, and surfaces. However, when a bias voltage is applied to the system, the DFT method cannot rigorously handle an open system under the nonperiodic and out of equilibrium conditions. Therefore, molecular electronics devices need to be taken into account by the Green's function formalism [44, 45]. Up to now, the combined density functional theory (DFT) and non-equilibrium Green's function (NEGF) methods have been widely used to study the quantum transport through nanoscale devices [46–49]. The great advantage of this method is its generality [50]: the transport properties of many different nanoscale materials, for example, molecular wires, nanotubes, graphene sheets and spintronic devices, etc., can be described under the same framework. The *I-V* characteristics are calculated without adjusting parameters, which is known as "first principles" or "*ab initio*" approach [51].

1.4 Outline of the thesis

This thesis presents the theoretical investigation of electronic structures and transport properties of molecular electronic devices. The computational framework is based on non-equilibrium Green's function (NEGF) formalism combined with density functional theory (DFT). The scientific work performed during PhD study is discussed, which lead to the papers in the list of publications.

The outline of this thesis is as follows. Chapter 2 introduces the electronic structure problem addressed by density functional theory (DFT) and includes the computational methods used in the numerical implementation. Chapter 3 describes the theoretical framework for the electron transport. We review the transport mechanisms in molecular devices, which will serve as the theoretical background of our studies. The basic Landauer and NEGF formalisms are introduced.

Chapter 4 contains a summary of the papers included in the thesis. The combined DFT-NEGF approach has been employed to investigate the electron transport properties of various molecular electronic devices:

• Carbon wires, one of the most attractive conducting molecular wires bridging two-dimensional electrodes, can provide a model for intercoupling molecular electronic circuit. The conduction mechanism of cumulene wires is described here. Two types of junctions have been considered: the cumulene wire connected to the gold leads via thiolate bonds (in Paper I) and the cumulene wire suspended between two carbon nanotubes (CNT) (in Paper II). Moreover, the stretched/compressed cumulene wires connected to the CNT leads causing a large variation in conductance have been discussed.

• Introducing switching functionality into molecular wires is one of the ways towards the practical application of molecular electronic devices. In paper III, we investigate the transport properties of a phthalocyanine molecule (H_2Pc). Two types of planar junctions are considered: the H_2Pc laterally connected to the cumulene wires and gold leads. The difference in conductance between the ON and OFF states, which is produced by the two tautomer configurations of H_2Pc molecule, is discussed from a theoretical point of view. In addition, the negative differential resistance (NDR) is revealed for the junction with gold leads.

• The molecular electronic devices can also be used as sensors. There has been recently developed a potential molecular electronics approach for fast DNA sequencing. Here, in Paper IV, we evaluate the performance of a graphene nanogap setup for the purpose of DNA sequencing application. Due to atomically thin graphene sheet, one can resolve the technical problem of achieving single-base resolution in electronic nucleobase detection. Furthermore, in Paper V, we have considered the effect of functionalization of the graphene edges which might offer some advantages over merely hydrogenated graphene edges for the purpose of DNA sequencing.

Finally, a summary is provided in Chapter 5.

2. Electronic Structure Methods

In this chapter, we will give a theoretical background of the density functional theory (DFT) and the computational methods, used for the electronic structure calculations in the thesis. Here, our aim is to provide a brief overview of the theory. Details of DFT can be found in many books and review articles [52–56].

2.1 Density Functional Theory

2.1.1 The many body problem

Well-defined collection of atoms forming molecules, solids, gases, liquids, etc. composes of electrons and nuclei. With quantum mechanics, we can describe a system of interacting electrons and nuclei by solving the Schrödinger equation

$$\hat{H}\Psi = E\Psi, \tag{2.1}$$

where E is the energy eigenvalue and the many-body hamiltonian operator is

$$\begin{aligned} \hat{H} &= \sum_{i=1}^{N_e} -\frac{\hbar^2}{2m}\nabla_i^2 + \sum_{I=1}^{N_{nuc}} -\frac{\hbar^2}{2M}\nabla_I^2 + \frac{1}{2}\sum_{i\neq j}\frac{e^2}{|\mathbf{r}_i - \mathbf{r}_j|} \\ &- \sum_{i,I}\frac{Z_I e^2}{|\mathbf{r}_i - \mathbf{R}_I|} + \frac{1}{2}\sum_{I\neq J}\frac{Z_I Z_J e^2}{|\mathbf{R}_I - \mathbf{R}_J|}. \end{aligned} \tag{2.2}$$

In the Eq. (2.2), the first and second terms are the kinetic energies of electrons and nuclei, and the last three terms are the electron-electron interactions, electron-nucleus interactions and nucleus-nucleus interactions, respectively. $\hbar$ is planck's constant, m and M are electron and nucleus mass, respectively. Z_I is the atomic number of the I^{th} atom, e is the electron charge, $\mathbf{r}_i$ and $\mathbf{R}_I$ are the positions of the i^{th} electron and I^{th} nucleus.

Solving the many-body Schrödinger equation is very complicated. To simplify the problem, Born-Oppenheimer approximation is used, stating that the nuclei are much heavier than the electrons and move much slowly than electrons. As a result, we can split the electronic and nuclear motions. The nuclei

are assumed to have fixed positions while the electrons are moving in the field of charged nuclei. The total wave function can be separated into electronic and ionic wave functions. Consequently, the Schrödinger equation for the electronic part is written as

$$\hat{H}_e(\mathbf{r},\mathbf{R})\Psi_e = E_e\Psi_e(\mathbf{r},\mathbf{R}), \tag{2.3}$$

with the electronic Hamiltonian given by

$$\hat{H}_e = \sum_{i=1}^{N_e} -\frac{\hbar^2}{2m}\nabla_i^2 + \frac{1}{2}\sum_{i\neq j}\frac{e^2}{|\mathbf{r}_i-\mathbf{r}_j|} + \hat{V}_{ext}, \tag{2.4}$$

where $\hat{V}_{ext}$ is the potential acting on the electrons due to the nuclei. Note that the interaction between nuclei enters as a parameter. Although the number of degrees of freedom of the system can be reduced by using Born-Oppenheimer approximation, solving the problem of the electron-electron interaction is still difficult. Moreover, the electronic wave function depends on all electron coordinates, but the number of electrons is considerably larger than the number of nuclei. As shown in the following section, it is more practical to use density functional description instead of the many-body wave functions. DFT requires less computational effort and gives a good description for the ground state properties of electronic systems.

2.1.2 The Hohenberg-Kohn theorems

The main concept of DFT is to describe the interacting system via the electron density instead of the many-body wave functions. DFT methods are founded on two fundamental theorems by Hohenberg and Kohn [57]. The first theorem is: *The ground state energy of a system of interacting electrons is a unique functional of the electronic charge density*. In other words, there exists a one-to-one correspondence between the ground-state wave function and the ground-state electron density.

The first Hohenberg-Kohn theorem only gives a proof of existence of functionals of the electron density. However, the true functional form is unknown. The second Hohenberg-Khon theorem, defining the property of the functional, is: *The electron density that minimizes the energy of the overall functional is the true ground-state electron density.*

According to these theorems, the expectation value of the Hamiltonian in Eq. (2.4) can be expressed as

$$< \psi|\hat{H}|\psi >= E[n(\mathbf{r})], \tag{2.5}$$

where $E[n(\mathbf{r})]$ is the total energy functional and $n(\mathbf{r})$ is the electron density. If the energy functional form is known, therefore, we can vary the electron density until the energy functional is minimized by using the variational principle:

$$\left.\frac{\delta E[n(\mathbf{r})]}{\delta n}\right|_{n=n_0} = 0. \tag{2.6}$$

From Eq. (2.6), the electron density corresponding to the minimum energy E_0 is the ground-state density, $n_0(\mathbf{r})$. Regarding to the first theorem, the ground-state energy can be expressed as

$$E_0 = <\psi_0|\hat{H}|\psi_0> = E[n_0(\mathbf{r})]. \tag{2.7}$$

2.1.3 Kohn-Sham equations

The way to reduce the original many-body problem into an auxiliary one-electron problem was proposed by Kohn and Sham [58]: interacting electrons are replaced into a non-interacting electrons moving in the effective potential. The total energy functional in Eq. (2.5) can be written as

$$E[n(\mathbf{r})] = T_0[n(\mathbf{r})] + \frac{1}{2}\int\int \frac{n(\mathbf{r})n(\mathbf{r}')}{|\mathbf{r}-\mathbf{r}'|} d\mathbf{r}d\mathbf{r}' + \int V_{ext}(\mathbf{r})n(\mathbf{r})d\mathbf{r} + E_{xc}[n(\mathbf{r})], \tag{2.8}$$

In the Eq. (2.8), $T_0[n(\mathbf{r})]$ is the kinetic energy functional of non-interacting electron system, the second term is the electrostatic energy or Hartree energy, the third term is the external energy due to nuclei, and the last term is all the remaining contribution to the energy, called the exchange and correlation energy.

By minimizing of Eq. (2.8) with respect to the density, we obtain the single-particle Kohn-Sham equations:

$$\left[-\frac{\nabla_i^2}{2} + V_{eff}(\mathbf{r})\right]\Psi_i(\mathbf{r}) = \varepsilon_i\Psi_i(\mathbf{r}), \tag{2.9}$$

where

$$V_{eff}(\mathbf{r}) = V_{ext} + \int \frac{n(\mathbf{r}')}{|\mathbf{r}-\mathbf{r}'|} d\mathbf{r} + \frac{\delta E_{xc}[n(\mathbf{r})]}{\delta n(\mathbf{r})}.$$

Note that the Kohn-Sham wave functions, $\Psi_i(\mathbf{r})$, do not give any direct physical meaning. They are just auxiliary functions for calculating the electron density. The electron density can be obtained from the Kohn-Sham wave functions,

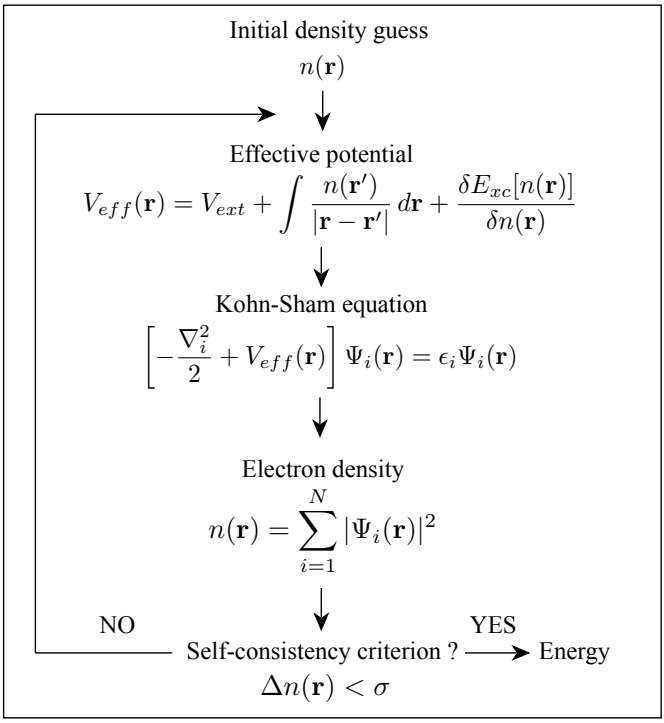

Figure 2.1: The schematic method of the self-consistency loop based on the Kohn-Sham equation.

$$n(\mathbf{r}) = \sum_{i=1}^{N} |\Psi_i(\mathbf{r})|^2. \tag{2.10}$$

In order to find the ground-state electron density, the Khon-Sham equations have to be solved self-consistently by iterative methods in the following algorithm (Fig. 2.1):

(1) An initial guess of electron density, $n(\mathbf{r})$, is defined.

(2) The effective potential, $V_{eff}(\mathbf{r})$, is calculated from the guess electron density.

(3) The Kohn-Sham equation is solved to obtain the Kohn-Sahm wave function, $\Psi_i(\mathbf{r})$.

(4) The electron density is calculated by using the Kohn-Sahm wave function.

(5) The calculated electron density is used as the initial density for next steps. Until the convergence of the electron density is reached, then we obtain the ground-state electron density, which is used in computing the energy, forces, stresses, etc.

2.1.4 Exchange-correlation functionals

The Kohn-Sham scheme has shown us how to transform the many-body problem into the effective single-electron problem. However, the exchange-correlation function, $E_{xc}[n(\mathbf{r})]$, need to be specified. Unfortunately, the exact form of the exchange-correlation functional is simply not known; hence, the approximation has to be done.

The simplest approximation is the so-called local density approximation (LDA) [58], derived from the exchange-correlation energy of the homogeneous electron gas. The LDA exchange-correlation functional is written as

$$E_{xc}^{LDA}[n(\mathbf{r})] = \int n(\mathbf{r})\varepsilon_{xc}^{hom} d\mathbf{r}, \tag{2.11}$$

where ε_{xc}^{LDA} is the exchange-correlation energy density of a homogeneous electron gas with the electron density, $n(\mathbf{r})$. Thus, the only information required is the exchange-correlation energy of the homogeneous electron gas, which can be derived exactly. Since the functional derived from the locally uniform electron gas, the error would be expected for quickly varying densities [53]. Although the LDA works very well for bulk solids, but it is better to use other functionals if the electron densities are not slowly varying, e.g., in atoms and molecules.

The way to obtain more accurate results has been made by considering more physical ingredients, i.e., the gradient of the electron density, the so-called Generalized Gradient Approximation (GGA). There have been many attempts to find a good functional form, two of the most commonly used functionals are the Perdew-Wang functional (PW91) [59] and the Perdew-Burke-Ernzerhof (PBE) [60]. In general, it is assumed that the GGA should provide better results than the LDA. However, this is not always true. In some cases, the results of LDA are better than that of the GGA when compared with experiments [61, 62].

2.2 Computational methods

So far, we have not described how to calculate the electronic structures based on DFT methods. SIESTA (Spanish Initiative for Electronic Simulations with Thousands of Atoms) code [63] has been chosen as a main tool for electronic structure calculations because the transport codes used in this thesis; TranSIESTA [48] and SMEAGOL [64, 65], use the SIESTA code as its DFT platform. The computational methods, employed in solving the Kohn-Sham equation, will be briefly described in this section.

2.2.1 The secular equation

To solve the Kohn-Shame equation, the Kohn-Sham wave function $\Psi_i(\mathbf{r})$ need to be expanded in a basis set of arbitrary basis functions, $\varphi_i(\mathbf{r})$, as

$$\Psi_i(\mathbf{r}) = \sum_{j=1}^{J} C_j^i \varphi_j(\mathbf{r}), \tag{2.12}$$

where C_j^i is a set of coefficients. Since the Kohn-Sham wave function is an infinite-dimensional space, J should be infinite. In practice, however, we always use a finite basis set; thus, $\Psi_i(\mathbf{r})$ cannot be exactly described. By replacing Eq. (2.12) into the Kohn-Sham equation Eq. (2.9), one can get

$$\sum_{j=1}^{J} C_j^i \left[-\frac{\nabla_i^2}{2} + V_{eff}(\mathbf{r}) \right] \varphi_j(\mathbf{r}) = \sum_{j=1}^{J} C_j^i \varepsilon_i \varphi_j(\mathbf{r}). \tag{2.13}$$

Multiplying with the conjugate of the basis function, $\varphi_k^*(\mathbf{r})$ and integrating over all real space, we have

$$\sum_{j=1}^{J} C_j^i \int \varphi_k^*(\mathbf{r}) \left[-\frac{\nabla_i^2}{2} + V_{eff}(\mathbf{r}) \right] \varphi_j(\mathbf{r})\, d\mathbf{r} = \sum_{j=1}^{J} C_j^i \varepsilon_i \int \varphi_k^*(\mathbf{r}) \varphi_j(\mathbf{r})\, d\mathbf{r}, \tag{2.14}$$

where $\int \varphi_k^*(\mathbf{r}) \left[-\frac{\nabla_i^2}{2} + V_{eff}(\mathbf{r}) \right] \varphi_j(\mathbf{r})\, d\mathbf{r}$ is the Kohn-Sham Hamiltonian matrix $\mathbb{H}$ and the overlap matrix $\mathbb{S}$ is $\int \varphi_k^*(\mathbf{r}) \varphi_j(\mathbf{r})\, d\mathbf{r}$. We can write Eq. (2.14) in the matrix form:

$$\mathbb{H}\mathbb{C} = \varepsilon \mathbb{S}\mathbb{C}, \tag{2.15}$$

which is known as the secular equation.

The Khon-Sham equations are now transformed into the secular equations written in matrix form. Thus, the Eq. (2.14) can be solved, which will lead to J eigenvalues and J sets of eigenfunctions.

2.2.2 Periodicity and k-point sampling

To solve Kohn-Sham equation Eq. (2.9), the appropriate boundary conditions need to be specified. The SIESTA code uses periodic boundary condition to simulate a supercell with replicating a unit cell in three dimensions. This is convenient for infinite and periodic systems such as bulk crystals. In addition, it can also be used to describe a finite system such as a molecule, placed in a sufficiently large unit cell. By using the supercell approach according to

the Bloch's theorem [66], the Kohn-Sham wave function can be written as a product of a wavelike part and a cell-periodic part, i.e.,

$$\Psi^n_{\mathbf{k}}(r) = u^n_{\mathbf{k}}(r)e^{i\mathbf{k}\cdot\mathbf{r}}, \tag{2.16}$$

where n is a discrete band index and $\mathbf{k}$ is a vector in the reciprocal space. This theorem shows that it is possible to map the Khon-Sham equation into the reciprocal space, and solve the equation for each value of $\mathbf{k}$ independently. In addition, one can use only possible values of $\mathbf{k}$ in the Brillouin zone. The integrated function $f(\mathbf{r})$ over the Brillouin zone can be written as

$$f(\mathbf{r}) = \frac{V_{cell}}{(2\pi)^3}\int_{BZ} F(\mathbf{k})d\mathbf{k} = \sum_j w_j F(k_j), \tag{2.17}$$

where $F(\mathbf{k})$ is the Fourier transform of $f(\mathbf{r})$, w_j is the weight factor and V_{cell} is the volume of a primitive cell in real space defined by the Wigner-Seitz construction. In SIESTA, the Monkhorst-pack method [67] is used for Brillouin-zone sampling. Note that a large supercell needs few k-points owing to the inverse relationship. Therefore, the Γ-point can be a reasonable approximation for the large supercell, which are considered here in the case of the DNA-graphene junction (Paper IV and Paper V).

2.2.3 Basis sets

Choosing an appropriate basis is essential to obtain accurate results. One possible choice of basis sets is a plane wave. For the periodic system, the plane-wave basis set appears to be the natural choice. There are several advantages of plane wave basis set; for example, the absence of basis set superposition error, the ability to control the accuracy with increasing the number of waves, and the high efficiency of using fast Fourier transform algorithm.

However, solving the Kohn-Sham equations using plane waves as the basis set has a high demand on the computational resource, resulting from the large number of plane waves needed to describe localized states. The plane waves are not centered at the nuclei but extended over all space. They also propagate across the whole cell, even there is no charge density. Consequently, the plane-wave basis sets are unsuitable for grid-based electronic structure calculations for a large system.

In SIESTA, solving the Kohn-Sham equation uses a linear combination of localized numerical atomic orbitals (LCAO) as the basis set. It can be written as products of a radial function and a spherical harmonic

$$\phi_{lmn}(r,\theta,\varphi) = R_{n,l}(r)Y_{l,m}(\theta,\varphi), \tag{2.18}$$

where $R_{n,l}$ is a radial function for orbital n and $Y_{l,m}$ is a real spherical harmonic for orbital angular momentum l and magnetic quantum number m, respectively. The radial function becomes zero beyond a certain radius.

Unlike plane waves, the accuracy of result for the given system depends on the basis size and shape. The number of basis functions can be expanded using a multiple-ζ basis set. Each ζ orbital corresponds to the same spherical harmonics but with different radial functions, i.e. single-ζ or "SZ", double-ζ or "DZ", triple-ζ or "TZ" for 1, 2 or 3 radial functions, etc. Moreover, it is possible to include polarization functions to account for the deformation induced by the bond formation in molecules or solids. The polarization function has the angular momentum one unit higher than the maximum occupied state in the atom; i.e., the p-orbitals can be used for polarizing s-orbitals, and the d-orbitals can be used for polarizing p-orbitals, etc. Adding polarization functions in the basis is denoted by "P", e.g., "DZP" for double ζ with polarization functions. The quality of basis sets can be checked by comparing energies and geometries at different levels, but DZP generally provides high-quality results with a reasonable computational cost for most of the systems.

2.2.4 Pseudopotential

Solving the Kohn-Sham equation would be simplified if we can decrease a computational burden due to core electrons. The core electrons do not play a significant role to define chemical bonding or other varying physical properties since these properties are described by valence electrons. The strong Coulomb potential and tightly bound core electrons in atoms are associated with rapidly varying wave functions with many nodes; therefore, a large number of basis functions need to be used to describe them.

The approach to reduce the number of basis functions is to use a pseudopotential. In generating the pseudopotential, there are two important steps. Firstly, core electrons are removed from the calculation and the ionic potential is replaced with the pseudopotential. Secondly, the full ionic potential, including the orthogonality of the valence wave functions to the core state, is replaced with a softer pseudopotential.

The theory of norm-conserving psudopotential has been proposed by Hamann, Schlüter, and Chiang [68]. The conditions for constructing the pseudotential are the following:

(1) The eigenvalues of the all-electron wave functions coincide with that of the pseudo wave functions for the chosen atomic reference configuration.

(2) The pseudo wave functions have to coincide with the all-electron wave function beyond the core radius, $r \geq r_c$.

(3) The pseudo wave functions are forced to have the same norm as the all-electron valence wave functions inside the cutoff radius, $r < r_c$.

(4) The logarithmic derivatives of the all electron and pseudo wave functions agree for $r \geq r_c$.

Several recipes have been now proposed to generate the first-principles pseudopotenials, which differ with the functional form of the potential and conditions of smoothing the pseudo-wave functions [69, 70]. In SIESTA, one generally uses norm-conserving pseudopotentials according to the Troullier-Martins parameterization [71], in the full non-local form of Kleinman-Bylander [72]. For more details, see the Ref. [63].

2.2.5 Geometry optimization

In all papers, geometrical optimizations have been performed to determine the stable configuration before calculating the transport properties. By using the Hellmann-Feynman theorem [52], one can calculate the force acting on the nuclei with ionic position $\mathbf{R}_I$:

$$F_I = -\frac{\partial \varepsilon}{\partial \mathbf{R}_I}, \tag{2.19}$$

where the total energy of the system ε can be written as

$$\varepsilon = \frac{<\Psi|\hat{H}|\Psi>}{<\Psi|\Psi>}. \tag{2.20}$$

ψ represents the Kohn-Sham wave function which is assumed to be normalized, thus $<\Psi|\Psi>$=1. From the calculated force acting on ions, they will be moved from one position to another to minimize the total energy. The Khon-Sham wave functions change due to the new ionic coordinates, resulting in the force on the ion. By substituting Eq. (2.20) into Eq. (2.19), we obtain

$$\begin{aligned} F_I &= -<\Psi|\frac{\partial \hat{H}}{\partial \mathbf{R}_I}|\Psi> - <\frac{\partial \Psi}{\partial \mathbf{R}_I}|\hat{H}|\Psi> - <\Psi|\hat{H}|\frac{\partial \Psi}{\partial \mathbf{R}_I}>, \\ &= -<\Psi|\frac{\partial \hat{H}}{\partial \mathbf{R}_I}|\Psi> - \varepsilon\left(\frac{\partial <\Psi|\Psi>}{\partial \mathbf{R}_I}\right), \\ &= -<\Psi|\frac{\partial \hat{H}}{\partial \mathbf{R}_I}|\Psi>. \end{aligned} \tag{2.21}$$

However, the Eq. (2.21) is not valid if the basis sets depend on the atomic positions. The error arises from the derivative of the basis set with respect to the ionic position, called the Pulay force. The Pulay forces are zero for the plane wave basis sets since the wave functions do not depend on the ionic positions. In contrast, the wave functions of localized basis sets are dependent on the atomic postions; thus, pulay corrections are needed.

2.3 Conclusion

DFT has now probably become the most popular and powerful method for studying electronic structures, which allows us to simulate very large systems with hundreds or thousands of atoms. To calculate the charge transport in the molecular devices, it is necessary to specify the atomic structure of molecules and binding at molecule–electrode interface. Since DFT provides an accurate description of the ground state properties, such as atomic structures, binding energies, lattice constants etc., it provides a good starting point for describing the charge transport in the molecular devices.

3. **Quantum transport theory**

3.1 Transport regimes

In the field of electron transport in mesoscopic and nanoscopic systems, different approaches have been used for each transport regime. Before setting up the transport calculation, therefore, we need to define the transport regime for given problems. Two characteristic lengths, used to distinguish the transport regime, are the momentum relaxation length, L_m, and the phase relaxation length, L_ϕ [73]. The momentum relaxation length (or electron mean free path) is the average distance which an electron can travel before its original momentum is lost, while the phase relaxation length is the average distance which an electron can travel until its original phase is destroyed. If the length of the device, L, is much longer than L_m and L_ϕ, the conductance is dependent on the length of the wire obeying the simple Ohm's law. That is the reason we called it as ohmic regime.

The development of electronic devices at a single-molecule scale has expanded existing theories of electrical transport beyond their limits. Due to small size of these devices, the quantum character of the electron need to be considered. The electron in quantum mechanics behaves like waves, which can show an interference effect. Under two characteristic lengths, we can divide the electron transport into three transport regimes:

(1) Ballistic transport regime, $\mathbf{L << L_m, L_\phi}$

In this transport regime, electrons can propagate freely from one lead to the other without scattering. There is no significant momentum and phase relaxation in the electron transport process through a device. The resistance can arise from the backscattered electron at the contact region. Ballistic conduction is typically observed in quasi-1D structures, such as metallic nanowires or carbon nanotubes, with quantized conductance ($G_0 = 2e^2/h$, where e is the electron charge and h is the Plank constant). The conductance of such a device is independent of its length. The ballistic transport has been considered here in the case of the cumulene wire studied in Paper I and Paper II.

(2) Elastic and coherent transport regime, $\mathbf{L < L_\phi}$

For a short molecule, electrons move too fast to interact with molecular vibration. As a result, the energy of electrons is conserved but the scattered wave functions do not lose their phase memory. The reduction of the transmission due to elastic scattering does not involve with L_ϕ but only with L_m. The res-

onant tunnelling phenomena in the molecular device studied in Paper III, VI, V occurs in this transport regime.

(3) Inelastic and incoherent transport regime, $\mathbf{L} > \mathbf{L}_\phi$

The incoherent transport regime can be generally observed in a long molecular bridge. Since the long traverse time of electrons, they can interact with other electrons or phonon that would constitute a phase-breaking or incoherent scattering process. Consequently, the phase of the electron waves is lost, in addition to the change of the electron momentum. The dynamic of the molecular chain plays a significant role in the transmission instead of the molecule-lead contact.

There are two approaches that have been widely used to study the transport problem: the Landauer method and the Non-Equilibrium Green's Function (NEGF) method. The Landauer approach allows us to describe the non-interacting electron transport corresponding to the ballistic or coherent transport regimes, while the NEGF approach is a more sophisticated method that can be used in all three transport regimes. In the following sections, we will briefly describe the the Landauer and NEGF methods used in studying the transport problems in this thesis.

3.2 Landauer approach

In the Landauer approach, we can imagine a system of two macroscopic leads connecting to the molecule or nanoscale structure. The system consists of a central region (C) sandwiched between left (L) and right (R) leads, connected to electron reservoirs. The left and right leads are kept at two, in general situation different, electrochemical potentials, μ_L and μ_R, where $\mu_L = \mu_R$ at zero applied voltage. The electrochemical potential difference between two leads causes the current flow. This difference is adjusted by applied bias voltage.

In such a geometrical model, the problem can be viewed as a scattering problem. An incident wave function, propagating along the central region, is scattered by a potential connecting to the two leads and then transmitted to the other lead. Landauer viewed the current flow as the probability of the electron to be transmitted from one lead to the other. Here, we will present a simple way to derive the Landauer formula, but still showing the important concept related to computational implementations. The rigorous derivation of this approach can be found in Ref. [74, 75].

Let us consider an ideal one-dimensional wire of length L between two leads. This system is assumed to be in the ballistic transport regime. In the 1D-wire, states in the direction normal to the propagation are quantized. The electron density per unit length corresponding to the given perpendicular state in the momentum range between k and $k + dk$, including spin is

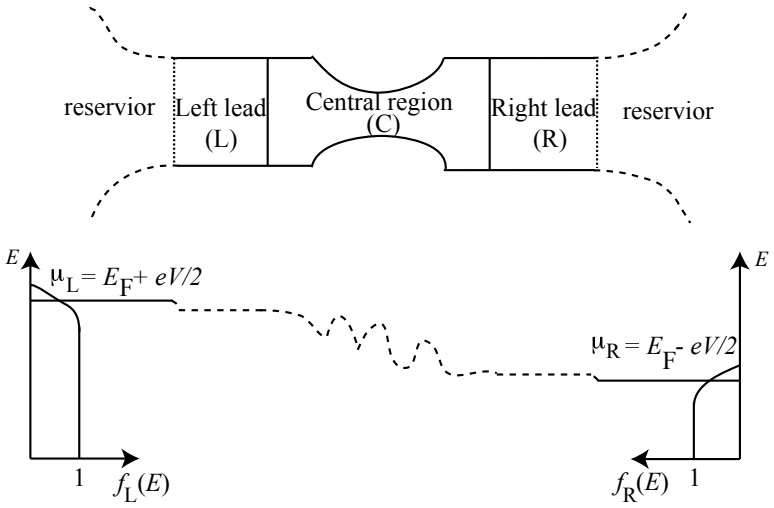

Figure 3.1: Schematic of the 'open system' described within the Landauer approach. The setup of the Landauer approach: left and right leads (L,R) are connected to two reservoirs held in equilibrium at two different electrochemical potentials (μ_L, μ_R). Both leads are connected to a central region (C), in which scattering can take place. The electrochemical potential is almost flat inside the leads, and the potential drop occurs across the junction. Adapted from ref. [74]

$$n(k)dk = 2\frac{1}{L}\frac{L}{2\pi}dk = 2\frac{1}{2\pi}f(k)dk, \tag{3.1}$$

where $f(k)$ is the Fermi distribution function.

At finite bias, the leads connected to reservoirs are in the equilibrium, where the Fermi distribution functions for the left and the right leads are $f_L(k)$ and $f_R(k)$, respectively. The current flowing through the system is

$$I = 2\int_0^\infty ev(k)n(k)dk = 2\int_0^\infty e\frac{\hbar k}{m_e}\left(\frac{f_L(k)}{2\pi} - \frac{f_R(k)}{2\pi}\right)dk, \tag{3.2}$$

where $v(k)$ is the electron velocity along the wire and m_e is the electron effective mass. At the zero temperature, the Fermi distributions are step functions, and the Eq. (3.2) becomes

$$I = 2\int_{\sqrt{2m_e\mu_R}/\hbar}^{\sqrt{2m_e\mu_L}/\hbar} e\frac{\hbar k}{m_e}\frac{1}{2\pi}dk = 2\frac{e^2}{h}\frac{\mu_L - \mu_R}{e} = 2\frac{e^2}{h}V_B, \tag{3.3}$$

where μ_L and μ_R are the electrochemical potential of the left and right leads, respectively. V_B is the bias voltage due to a shift in the electrochemical potentials of both leads, where $\mu_L - \mu_R = eV_B$.

From the Eq. (3.3), the maximum conductance of a one conduction channel with two spin states, G_0, is

$$G_0 = \frac{2e^2}{h} = (12.9k\Omega)^{-1}. \tag{3.4}$$

This is the so-called quantum of conductance.

Generally, the nanodevice and its connection to the leads is not ideal due to scattering. Therefore, the formula for the conductance can be written as

$$G = \frac{2e^2}{h} T(E_F), \tag{3.5}$$

where E_F is the Fermi energy of the system.

The Eq (3.4) is used for the 1D wire, where there is only one conducting mode in the direction normal to the propagation. For the finite width device, the number of quantum modes carrying electrons is to be considered. The Landauer formula can be generalized to

$$G = \frac{2e^2}{h} \sum_{i,j} T_{ij}(E_F), \tag{3.6}$$

where T_{ij} is the probability of electrons passing from i^{th} conducting mode at the left of the device to the j^{th} conducting mode at the right of the device. More generally, the current at a finite bias can be expressed as

$$I = \frac{2e}{h} \int_{-\infty}^{\infty} T(E,V_b)[f(E-\mu_L) - f(E-\mu_R)]dE \tag{3.7}$$

According to Landauer formula, Eq. (3.7), only one ingredient required is the energy dependent transmission function. This is typically derived from the Green's function of the central region connected to both leads, as we will discuss in the following section.

3.3 Non-equilibrium Green function (NEGF)

The study of electron transport is modelled on the atomic level; therefore, combining the NEGF method with DFT has a great advantage over other methods. Details of the NEGF method are described in many books and articles [44, 45, 74, 76, 77]. Here, we will give a general description of the NEGF method to calculate current-voltage characteristics of molecular devices.

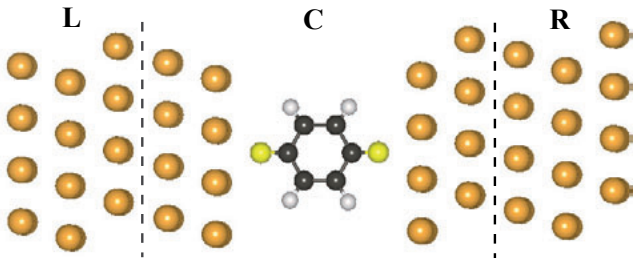

Figure 3.2: Schematic illustration of a two-probe system containing a molecule connected to left (L) and right (R) leads.

We start from the screening approximation, dividing the system into the central region, left and right leads, then the Hamiltonian of the system is determined. By using the NEGF approach, the charge density is calculated in a self-consistent manner. The wave function in each region corresponding to an incoming wave function is described. The section ends with a description on how one calculates the electron current with the NEGF method.

3.3.1 Screening approximation

Fig.3.2 illustrates a two-probe system, partitioned into three parts: the semi-infinite left (L) and right (R) leads coupled with the central region (C). The semi-infinite lead has a regular periodic structure in the direction of the transport, resulting in the infinite dimension of the Hamiltonian. Using a screening approximation, we can divide the effective potential and charge density into the central region and left/right lead region treated as a bulk system. The surface effects due to the perturbation of a molecule at the contact, i.e. the charge transfer, atomic relaxation and the potential disturbance, are eliminated by including a few layer of leads to the central region, that effectively screen them from the bulk of the electrodes.

Using the screening approximation, we can express the total Hamiltonian as

$$\begin{pmatrix} \mathbf{H}_L & \tau_L & 0 \\ \tau_L^\dagger & \mathbf{H}_C & \tau_R^\dagger \\ 0 & \tau_R & \mathbf{H}_R \end{pmatrix}, \tag{3.8}$$

where $\mathbf{H_L}$, $\mathbf{H_C}$ and $\mathbf{H_R}$ denote the Hamiltonian matrices of the left, central and right parts, respectively. $\tau_{(L)R}$ is the matrix involving the interaction between the left(right) lead and the central region. We assume that there is no direct tunnelling between leads L and R.

After partitioning the open system into different regions, the next step is to solve the Schrödinger equation. The Non-equilibrium Green function (NEGF) approach is used to solve the Schrödinger equation, described in the following section.

3.3.2 Green's functions and self energies

The retarded Green's function $\mathbf{G}$ corresponding to the Hamiltonian matrix $\mathbf{H}$ is defined as

$$[E^+\mathbf{S}-\mathbf{H}]\mathbf{G}=\mathbf{I}, \tag{3.9}$$

where $E^+=\lim_{\eta\to 0^+}E+i\eta$, $\mathbf{S}$ is an overlap matrix, and $\mathbf{I}$ is an infinitely-dimensional identity matrix. By substituting the Hamiltonian matrix of the system given by Eq. (3.8) into the Eq. (3.9), we have

$$\begin{pmatrix} E^+\mathbf{S}_L-\mathbf{H}_L & -\tau_L & 0 \\ -\tau_L^\dagger & E^+\mathbf{S}_C-\mathbf{H}_C & -\tau_R^\dagger \\ 0 & -\tau_R & E^+\mathbf{S}_R-\mathbf{H}_R \end{pmatrix} \begin{pmatrix} \mathbf{G}_L & \mathbf{G}_{LC} & 0 \\ \mathbf{G}_{CL} & \mathbf{G}_C & \mathbf{G}_{CR} \\ 0 & \mathbf{G}_{RC} & \mathbf{G}_R \end{pmatrix}$$

$$= \begin{pmatrix} \mathbf{I} & 0 & 0 \\ 0 & \mathbf{I} & 0 \\ 0 & 0 & \mathbf{I} \end{pmatrix}. \tag{3.10}$$

We consider the three equations in the second column:

$$(E^+\mathbf{S}_L-\mathbf{H}_L)\mathbf{G}_{LC}-\tau_L\mathbf{G}_C = 0 \tag{3.11}$$

$$-\tau_L^\dagger\mathbf{G}_{LC}+(E^+\mathbf{S}_C-\mathbf{H}_C)\mathbf{G}_C-\tau_R^\dagger\mathbf{G}_{RC} = \mathbf{I} \tag{3.12}$$

$$(E^+\mathbf{S}_R-\mathbf{H}_R)\mathbf{G}_{RC}-\tau_R\mathbf{G}_C = 0. \tag{3.13}$$

From solving the Eq. (3.11) and Eq. (3.13), we obtain

$$\mathbf{G}_{LC}=\mathbf{g}_L\tau_L\mathbf{G}_C \tag{3.14}$$

and

$$\mathbf{G}_{RC}=\mathbf{g}_R\tau_R\mathbf{G}_C, \tag{3.15}$$

where $\mathbf{g}_{L/R}=(E^+\mathbf{S}_{L/R}-\mathbf{H}_{L/R})^{-1}$ is the "surface Green's function" of the left/right lead uncoupled to the central region.

Substituting the Eq. (3.14) and Eq. (3.15) into the Eq. (3.12), we get

$$-\tau_L^\dagger\mathbf{g}_L\tau_L\mathbf{G}_C+(E^+\mathbf{S}_C-\mathbf{H}_C)\mathbf{G}_C-\tau_R^\dagger\mathbf{g}_R\tau_R\mathbf{G}_C=\mathbf{I}. \tag{3.16}$$

Then, the final expression for the retarded Green's function of the central region can be expressed as

$$\mathbf{G}_C = [E^+\mathbf{S}_C - \mathbf{H}_C - \mathbf{\Sigma}_L(E) - \mathbf{\Sigma}_R(E)]^{-1}, \tag{3.17}$$

where

$$\mathbf{\Sigma}_L(E) = \boldsymbol{\tau}_L^\dagger \mathbf{g}_L \boldsymbol{\tau}_L \tag{3.18}$$

and

$$\mathbf{\Sigma}_R(E) = \boldsymbol{\tau}_R^\dagger \mathbf{g}_R \boldsymbol{\tau}_R. \tag{3.19}$$

We call $\mathbf{\Sigma}_{L/R}$ a "self-energy". The self-energy is associated to the energy level shift Δ and the energy level broadening Γ, shown in Fig. 3.3. The energy level shift and the energy level broadening are derived from the real part

$$\Delta_{L/R}(E) = \mathrm{Re}\Sigma_{L/R}(E) \tag{3.20}$$

and the imaginary part

$$\Gamma_{L/R}(E) = i[\Sigma_{L/R}(E) - \Sigma_{L/R}^\dagger(E)] \tag{3.21}$$

$$= -2\mathrm{Im}[\Sigma_{L/R}(E)] \tag{3.22}$$

of the self-energy, respectively. In addition, the broadening of the molecular level is also associated with the lifetime of electronic states on molecules. When the molecule is coupled to the leads, electrons can escape into the right or left leads, and spend time in the state localized at the central region. The lifetime of state is inversely proportional to the broadening of electrons: $\tau_{L,R}\Gamma = \hbar$.

Regarding to the Eq. (3.17), the infinite-dimensional Hamiltonian is reduced to the dimension of the central part, where the self-energies, $\Sigma_L(E)$

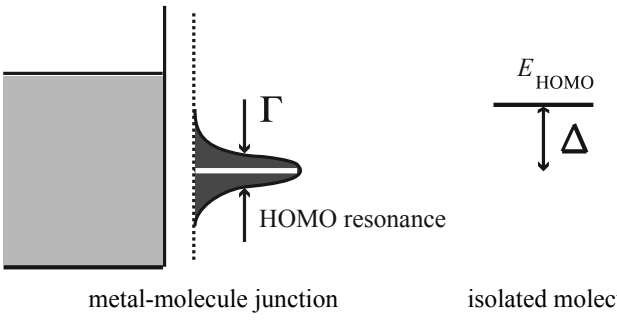

Figure 3.3: When the molecule is attached to semi-infinite leads, its energy levels are shifted by Δ. The energy level broadening due to the coupling to the contact is given by Γ.

and $\Sigma_R(E)$, include all information of the semi-infinite properties of the leads. The central part directly interacts only with the finite part of the right and left leads. Consequently, we can focus on only the Green's function matrix of the central region and treat the effect of semi-infinite leads in the term of effective interaction. The effective Hamiltonian can be expressed as

$$\mathbf{H_{eff}} = \mathbf{H_C} + \mathbf{\Sigma}_L(E) + \mathbf{\Sigma}_R(E). \tag{3.23}$$

3.3.3 Charge density matrix

Let us first introduce the spectral function:

$$A(E) = i(G - G^\dagger), \tag{3.24}$$

where the Green function can be expanded in the eigenbasis:

$$G = \int_k \frac{|\psi_k\rangle\langle\psi_k|}{E + i\eta - E'_k}. \tag{3.25}$$

Substituting the Eq. (3.25) into the Eq. (3.24), we get

$$\begin{aligned} A(E) &= i\int |\psi_k\rangle\langle\psi_k| \left(\frac{1}{E + i\eta - E'_k} - \frac{1}{E - i\eta - E'_k}\right) \\ &= \int |\psi_k\rangle\langle\psi_k| \frac{2\eta}{(E - E'_k)^2 + \eta^2}. \end{aligned} \tag{3.26}$$

We let η go to zero, therefore

$$A(E) = 2\pi \int dk \delta(E - E'_k) |\psi_k\rangle\langle\psi_k|, \tag{3.27}$$

where $\delta(E - E'_k)$ is the delta function.

In general, the delta function can be used to represent the density of states (DOS) of the level E_k, consequently, the Eq. (3.27) can be expressed as

$$A(E) = 2\pi \mathrm{DOS}(E) |\psi_k\rangle\langle\psi_k|. \tag{3.28}$$

From the Eq. (3.21), Eq. (3.24) and Eq. (3.17), we can also write the spectral function:

$$\begin{aligned} A_C(E) &= i(G_C - G_C^\dagger) = iG_C({G_C^\dagger}^{-1} - G_C^{-1})G_C^\dagger \\ &= iG_C(E - H_C - \Sigma_L^\dagger(E) - \Sigma_R^\dagger(E) - E + H_C + \Sigma_L(E) + \Sigma_R(E))G_C^\dagger \\ &= G(\Gamma_L(E) + \Gamma_R(E))G^\dagger = A_L(E) + A_R(E). \end{aligned} \tag{3.29}$$

By using the Eq. (3.28) and Eq. (3.29), we can evaluate different system properties, for example, the charge density matrix $\mathbf{D_C}$ from the Green function of the central region:

$$\mathbf{D_C} = \int_{-\infty}^{\infty} \frac{dE}{2\pi}[f(E-\mu_L)\mathbf{A}_L(E) + f(E-\mu_R)\mathbf{A}_R(E)] \tag{3.30}$$

$$= \int_{-\infty}^{\infty} \frac{dE}{2\pi}[f(E-\mu_L)(\mathbf{G}_C\Gamma_L\mathbf{G}_C^{\dagger})(E) + f(E-\mu_R)(\mathbf{G}_C\Gamma_R\mathbf{G}_C^{\dagger})(E)], \tag{3.31}$$

where f denotes the occupation of the state with energy E and $\mu_{L/R}$ is the chemical potential of the left/right lead. It follows that the total density $\mathbf{D_C}$ is a sum of densities induced from each electrode, proportional to the $(\mathbf{G}_C\Gamma_R\mathbf{G}_C^{\dagger})(E)$ and $(\mathbf{G}_C\Gamma_L\mathbf{G}_C^{\dagger})(E)$.

In the equilibrium, we can combine the left and the right part of the Eq. (3.31), then we have

$$\mathbf{D_C} = \int_{-\infty}^{\infty} \frac{dE}{2\pi}[f(E-\mu)(\mathbf{G}_C(\Gamma_L(E)+\Gamma_R(E))\mathbf{G}_C^{\dagger})(E)], \tag{3.32}$$

where $\mathbf{G}_C(\Gamma_L(E)+\Gamma_R(E))\mathbf{G}_C^{\dagger}$ can be evaluated by using Eq. (3.29);

$$\begin{aligned}\mathbf{G}_C(\Gamma_L(E)+\Gamma_R(E))\mathbf{G}_C^{\dagger} &= i\mathbf{G}[\Sigma_L(E)-\Sigma_L(E)^{\dagger}+\Sigma_R(E)-\Sigma_R(E)^{\dagger}]\mathbf{G}^{\dagger} \\ &= -i\mathbf{G}[(\mathbf{G}^{-1})-(\mathbf{G}^{\dagger})^{-1}]\mathbf{G}^{\dagger} \\ &= 2\mathrm{Im}[\mathbf{G}_C].\end{aligned} \tag{3.33}$$

By substituting the Eq. (3.32) into the Eq. (3.33), the charge density given by the Eq. (3.31) is reduced to the well-known expression:

$$\mathbf{D}_C = -\frac{1}{\pi}\int_{-\infty}^{\infty} \mathrm{Im}[\mathbf{G}_C(E)f(E-\mu)]dE. \tag{3.34}$$

In the same manner with the NEGF method, one can calculate matrix density of states $\mathbf{D}$ as

$$\mathbf{D} = -\frac{1}{\pi}\int_{-\infty}^{\infty} \mathrm{Im}[\mathbf{G}_C(E)]dE. \tag{3.35}$$

It is customary to write the density in the term of lesser Green's function

$$\mathbf{D} = -i\int_{-\infty}^{\infty} \frac{dE}{2\pi}\mathbf{G}_C^{<}(E), \tag{3.36}$$

where $\mathbf{G}_C^{<}(E) = -2i\mathrm{Im}[\mathbf{G}_C(E)]$.

As discussed above, for the system in equilibrium, we assume to a single electrochemical potential. In the non-equilibrium, as shown in Fig.3.4, the system is biased resulting in the difference in the electrochemical potential of

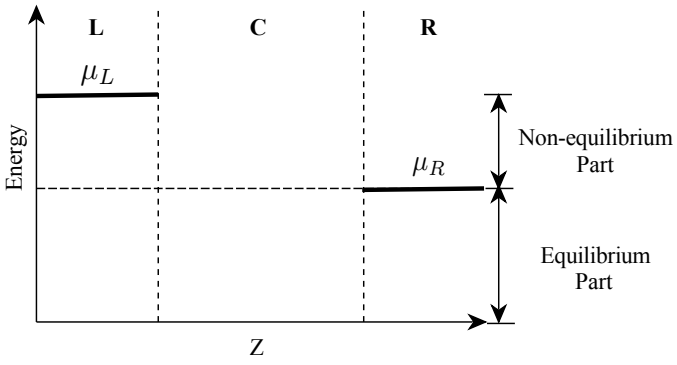

Figure 3.4: Schematic drawing of system driven out of the equilibrium by a bias voltages, $V_B = (\mu_L - \mu_R)/e$.

the left and right lead, μ_L and μ_R. In the non-equilibrium, we can divide the density matrix into two parts

$$\mathbf{D}_C = \mathbf{D}_C^{eq} + \mathbf{D}_C^{neq}, \tag{3.37}$$

where $\mathbf{D}^{eq}$ and $\mathbf{D}^{neq}$ correspond to the density matrix of the equilibrium part and the non-equilibrium part, respectively. $\mathbf{D}^{eq}$ is the density at the equilibrium region where energies of electrons range below both electrochemical potentials. The calculation of $\mathbf{D}^{eq}$ can be obtained in the same way with the density matrix calculation of the equilibrium system. From the Eq. (3.34), we can write the charge density of the equilibrium part as

$$\mathbf{D}_C^{eq} = -\frac{1}{\pi}\int_{E_B}^{\infty} \mathrm{Im}\mathbf{G}_C(E) f(E-\mu_R), \tag{3.38}$$

where E_B is the bottom energy of occupied states.

The electron density at the non-equilibrium region, in which energies of electrons range between the bias window, is given by

$$\mathbf{D}_C^{neq} = \frac{1}{2\pi}\int_{-\infty}^{\infty} dE \Big[\mathbf{G}_C(E)\Gamma_R(E)\mathbf{G}^{\dagger}{}_C(E)[f(E-\mu_L) - f(E-\mu_R)\Big]. \tag{3.39}$$

For the equilibrium part, the integral in Eq. (3.38) can easily be calculated by using complex contour integration. We need to define the bottom energy of occupied states, E_B, which is the value for the lower limit of integration. This value has to be chosen to include all occupied states of the system. However, $\mathbf{D}^{neq}$ is not analytic. Thus, the integral must be evaluated along the real axis using a dense set of integration points. $\mathbf{D}^{neq}$ is bound by the Fermi functions

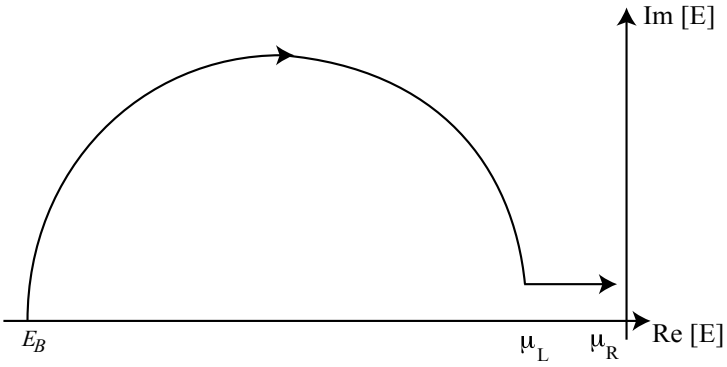

Figure 3.5: Diagram of the integration path used to calculate the non-equilibrium charge density. E_B is the bottom energy of occupied states. The integral is performed along the semicircular path in the imaginary axis for the equilibrium part, and along the real energy axis for the non-equilibrium part.

of the left and right leads, and the integration is performed in the energy range between the two electrochemical potentials. The schematic drawing of the Green function integration leading to the non-equilibrium charge density is illustrated in Fig. 3.5.

Finally, we can calculate the electron density in space

$$\rho(\mathbf{r}) = \sum_{\alpha\beta} \phi_\alpha(\mathbf{r})(\mathbf{D}_C)_{\alpha\beta}\phi_\beta(\mathbf{r}), \tag{3.40}$$

where $\phi_{\alpha/\beta}$ is a localized atomic basis orbital.

The electron density is calculated in a self-consistent manner, as shown in Fig.3.6. Here, we combine the NEGF formalism with DFT. The Hamiltonian is derived from the DFT procedure, and the electron density for an open system is calculated with the NEGF technique. The retarded Green's function based on the Hamiltonian is defined, while the Hamiltonian is a functional of the electron density itself. The problem is usually treated in an iterative way until convergence is achieved.

3.3.4 Response to an incoming wave

In this section, we will derive the wave functions corresponding to incoming waves in each region; Ψ_L, Ψ_C and Ψ_R. By using the screening approximation, the Schrödinger equation can be written as

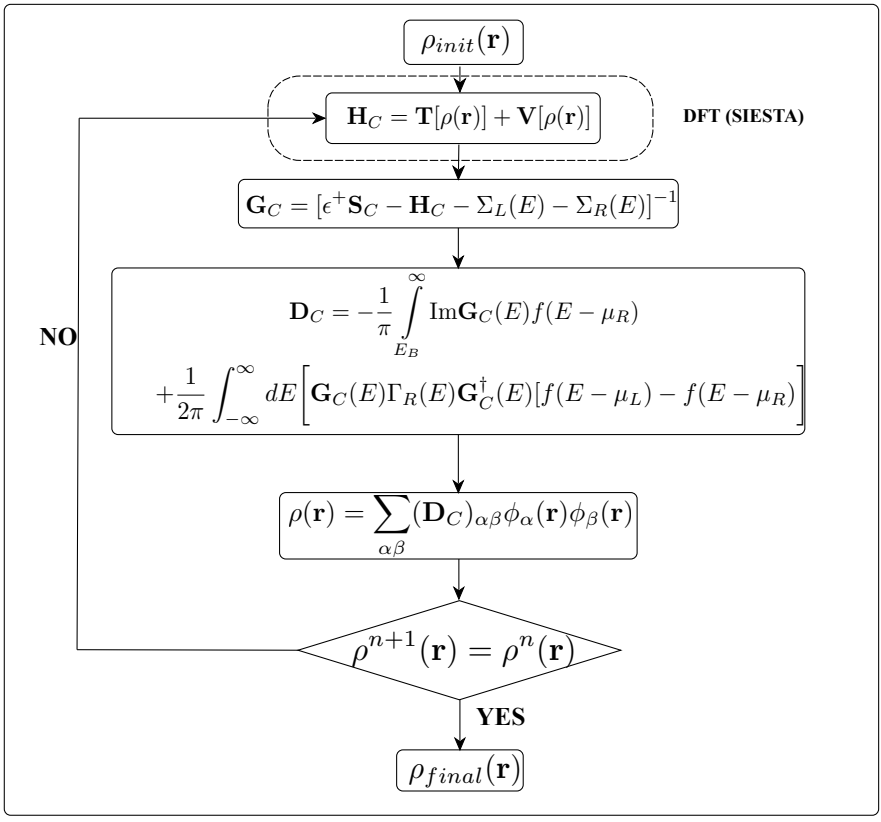

Figure 3.6: The schematic form of the self-consistency loop based on the NEGF+DGF method.

$$\begin{pmatrix} \mathbf{H}_L & \tau_L & 0 \\ \tau_L^\dagger & \mathbf{H}_C & \tau_R^\dagger \\ 0 & \tau_R & \mathbf{H}_R \end{pmatrix} \begin{pmatrix} |\psi_L\rangle \\ |\psi_C\rangle \\ |\psi_R\rangle \end{pmatrix} = E\mathbf{S} \begin{pmatrix} |\psi_L\rangle \\ |\psi_C\rangle \\ |\psi_R\rangle \end{pmatrix}. \tag{3.41}$$

We first consider the isolated left contact, where an incoming wave is totally reflected at the end of the contact. These solutions are denoted with $|\nu\rangle$. The isolated left contact can be a part of the whole system with $\tau_L = 0$, then we have

$$\begin{pmatrix} \mathbf{H}_L & 0 & 0 \\ 0 & \mathbf{H}_C & \tau_R^\dagger \\ 0 & \tau_R & \mathbf{H}_R \end{pmatrix} \begin{pmatrix} |\nu\rangle \\ |0\rangle \\ |0\rangle \end{pmatrix} = E'\mathbf{S} \begin{pmatrix} |\nu\rangle \\ |0\rangle \\ |0\rangle \end{pmatrix}. \tag{3.42}$$

Connecting the left contact to the central region, we can calculate the wave function of the whole system. The anzats $|\Psi\rangle + |\nu\rangle$ is put into the Schrödinger equation:

$$\begin{pmatrix} \mathbf{H}_L & \tau_L & 0 \\ \tau_L^\dagger & \mathbf{H}_C & \tau_R^\dagger \\ 0 & \tau_R & \mathbf{H}_R \end{pmatrix} \begin{pmatrix} |\Psi_L\rangle + |\nu\rangle \\ |\Psi_C\rangle \\ |\Psi_R\rangle \end{pmatrix} = E'\mathbf{S} \begin{pmatrix} |\Psi_L\rangle + |\nu\rangle \\ |\Psi_C\rangle \\ |\Psi_R\rangle \end{pmatrix}. \tag{3.43}$$

From Eq. (3.42) and Eq. (3.43), one can get

$$\begin{pmatrix} \mathbf{H}_L & \tau_L & 0 \\ \tau_L^\dagger & \mathbf{H}_C & \tau_R^\dagger \\ 0 & \tau_R & \mathbf{H}_R \end{pmatrix} |\Psi\rangle + \begin{pmatrix} 0 & \tau_L & 0 \\ \tau_L^\dagger & 0 & 0 \\ 0 & 0 & 0 \end{pmatrix} \begin{pmatrix} |\nu\rangle \\ |0\rangle \\ |0\rangle \end{pmatrix} = E\mathbf{S}|\Psi\rangle +$$

$$(E - E')\mathbf{S} \begin{pmatrix} |\nu\rangle \\ |0\rangle \\ |0\rangle \end{pmatrix}. \tag{3.44}$$

Then, the Schrödinger equation can be written in the following form:

$$\begin{pmatrix} \mathbf{H}_L & \tau_L & 0 \\ \tau_L^\dagger & \mathbf{H}_C & \tau_R^\dagger \\ 0 & \tau_R & \mathbf{H}_R \end{pmatrix} |\Psi\rangle = E\mathbf{S}|\Psi\rangle - \begin{pmatrix} (E - E')\mathbf{S}|\nu\rangle \\ \tau_L^\dagger|\nu\rangle \\ |0\rangle \end{pmatrix}. \tag{3.45}$$

According to the Eq. (3.45), we can write the wave function of the central part due to the incoming wave as

$$|\Psi_C\rangle = \mathbf{G}_C \tau_L^\dagger |v\rangle . \tag{3.46}$$

From the Eq. (3.41), we find

$$\begin{aligned} \mathbf{H}_R |\Psi_R\rangle + \tau_R |\Psi_C\rangle &= E\mathbf{S} |\Psi_C\rangle & (3.47)\\ |\Psi_R\rangle &= \mathbf{g}_R \tau_R |\Psi_C\rangle . & (3.48) \end{aligned}$$

By substituting the Eq. (3.46) into the Eq. (3.48), the wave function of the right lead due to the incoming wave is expressed as

$$|\Psi_R\rangle = \mathbf{g}_R \tau_R \mathbf{G}_C \tau_L^\dagger |v\rangle . \tag{3.49}$$

To calculate the wave function of the left lead containing the incoming wave, we need to add the incoming wave, yielding the expression:

$$|\Psi_L\rangle = (1 + \mathbf{g}_L \tau_L \mathbf{G}_C \tau_L^\dagger) |v\rangle . \tag{3.50}$$

3.3.5 Calculating the current

Let us first describe the probability current to find the electron flowing in the system. This can be derived from the continuity equation, using two contacts. In the steady state, the current probability does not change over time:

$$\begin{aligned} 0 &= \frac{\partial \langle \psi_C \mid \psi_C \rangle}{\partial t} & (3.51)\\ &= \frac{\partial |\psi_C\rangle}{\partial t} \langle \Psi_C | + |\Psi_C\rangle \frac{\partial \langle \Psi_C |}{\partial t}. & (3.52) \end{aligned}$$

The time-dependent Schrödinger equation is defined as

$$\frac{\partial |\Psi\rangle}{\partial t} = -\frac{i}{\bar{h}} H |\Psi\rangle . \tag{3.53}$$

Using the Eq. (3.41) and Eq. (3.53), we have

$$\frac{\partial |\Psi_C\rangle}{\partial t} = \frac{i}{\bar{h}} (\tau_L^\dagger |\Psi_L\rangle + H_C |\Psi_C\rangle + \tau_R^\dagger |\Psi_R\rangle). \tag{3.54}$$

Inserting the Eq. (3.54) into the Eq. (3.52), one can get

$$0 = -\frac{i}{\bar{h}} ([- \langle \Psi_L | \tau_L |\Psi_C\rangle + \langle \Psi_C | \tau_L^\dagger |\Psi_L\rangle] + [\langle \Psi_C | \tau_R^\dagger |\Psi_R\rangle - \langle \Psi_R | \tau_R |\Psi_C\rangle]) \tag{3.55}$$

Regarding to the Eq. (3.55), we can interpret the first bracket as the term of incoming probability current from the contact L and the second bracket as that from the contact R. Now, we can write the electric current from an arbitrary contact j into the central region as the charge times the probability current:

$$i_j = \frac{ie}{\bar{h}}(\langle\Psi_C|\,\tau_j\,|\Psi_j\rangle - \langle\Psi_j|\,\tau_j^\dagger\,|\Psi_C\rangle), \tag{3.56}$$

where $j = L,R$

To calculate the electric current, the wave function of the contact $|\Psi_j\rangle$ and central $|\Psi_C\rangle$ parts is put into the Eq. (3.56). Substituting the wave function from the Eq. (3.46) and Eq. (3.49) into the Eq. (3.56), the current through the system due to the incoming wave is

$$\begin{aligned} i_{R\text{ from }\nu} &= \frac{ie}{\bar{h}}(\langle\nu|\,\tau_L\mathbf{G}_C^\dagger\tau_R^\dagger\mathbf{g}_R\tau_R\mathbf{G}_C\tau_L^\dagger\,|\nu\rangle - \langle\nu|\,\tau_L\mathbf{G}_C^\dagger\tau_R^\dagger\mathbf{g}_R^\dagger\tau_R\mathbf{G}_C\tau_L^\dagger\,|\nu\rangle) \\ &= \frac{ie}{\bar{h}}(\langle\nu|\,\tau_L\mathbf{G}_C^\dagger\tau_R^\dagger(\mathbf{g_R} - \mathbf{g_R}^\dagger)\tau_R\mathbf{G}_C\tau_L^\dagger\,|\nu\rangle) \\ &= \frac{e}{h}\,\langle\nu|\,\tau_L\mathbf{G}_C^\dagger\Gamma_R\mathbf{G}_C\tau_L^\dagger\,|\nu\rangle\,. \end{aligned} \tag{3.57}$$

Since there are several modes in the contact, we will denote the incoming wave as $|\nu_n\rangle$, where n is a quantum number. To obtain the total current through the device, we need to sum over the incoming states and integrate over the energy E. The total current through the device is

$$\begin{aligned} I_{\text{R from L}} &= \frac{2e}{\bar{h}}\int_{-\infty}^{\infty} dE \sum_n \text{DOS}(E)\,\langle\nu_n|\;\tau_L\mathbf{G}_C^\dagger\Gamma_R\mathbf{G}_C\tau_L^\dagger\,|\nu_n\rangle \\ &= \frac{2e}{\bar{h}}\int_{-\infty}^{\infty} dE \sum_{m,n} \text{DOS}(E)\,\langle\nu_n|\,\tau_L\,|m\rangle\,\langle m|\,\mathbf{G}_C^\dagger\Gamma_R\mathbf{G}_C\tau_L^\dagger\,|\nu_n\rangle \\ &= \frac{2e}{\bar{h}}\int_{-\infty}^{\infty} \sum_m \langle m|\,\mathbf{G}_C^\dagger\Gamma_R\mathbf{G}_C\tau_L^\dagger(\sum_n \text{DOS}(E)\,|\nu_n\rangle\,\langle\nu_n|)\tau_L\,|m\rangle \\ &= \frac{2e}{\bar{h}}\int_{-\infty}^{\infty} \sum_m \langle m|\,\mathbf{G}_C^\dagger\Gamma_R\mathbf{G}_C\tau_L^\dagger\frac{A_L}{2\pi}\tau_L\,|m\rangle \\ &= \frac{e}{\pi\bar{h}}\int_{-\infty}^{\infty} \text{Tr}(\mathbf{G}_C^\dagger\Gamma_R\mathbf{G_C}\Gamma_L), \end{aligned} \tag{3.58}$$

where a spin factor of 2 is included.

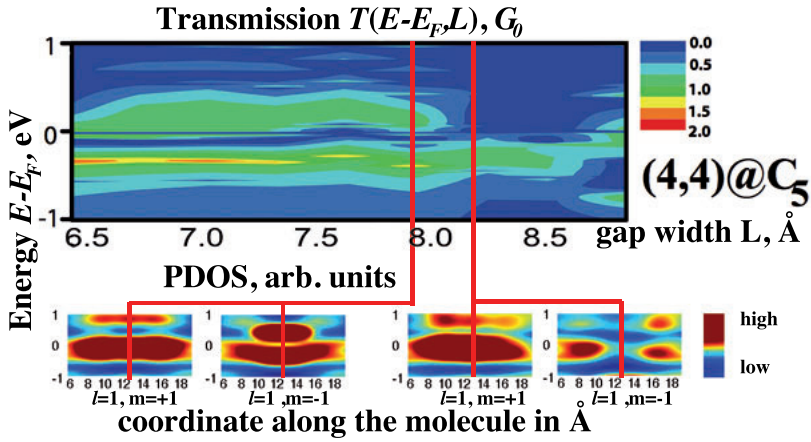

Figure 3.7: Zero-bias transmission on the energy-length plane T(E=0, L) and corresponding projected density of $p_{m=1}$ and $p_{m=-1}$ states for the carbon atomic wire stretched between two CNT electrodes at the two lengths corresponding to the II(C) and II(P) configurations as indicated in the Fig. 4.4.

With the reservoir connected to the contact, the states are filled according to the Fermi distribution. Finally, the current through the device connected to two contacts at chemical potential μ_R and μ_L is written as

$$I = \frac{e}{\pi\bar{h}} \int_{-\infty}^{\infty} \mathrm{Tr}(\mathbf{G}_C^{\dagger}\Gamma_R\mathbf{G}_\mathbf{C}\Gamma_L)(f(E-\mu_L) - f(E-\mu_R)), \tag{3.59}$$

which has the same form as the Landauer formula, Eq. (3.7). Thus, we can associate

$$T(E) = [\mathbf{G}_C^{\dagger}\Gamma_R\mathbf{G}_\mathbf{C}\Gamma_L], \tag{3.60}$$

with the transmission coefficient.

To elucidate the properties of transmission, we can compare the Eq. (3.60) and Eq. (3.39). Finite transmission probability will be found only when the density induced from either electrodes is finite. However, this is the necessary, but not sufficient condition to have finite transmission, because the scattering at the opposite electrode can significantly decrease the transmission function. This is expressed in Eq. (3.60) in the form of the $\Gamma_{(L/R)}$ factor, which describes the coupling to the corresponding electrode. On the other hand, if the coupling is good, it is only the matter of having sufficient density of states in the central region to obtain conducting system with high $T(E)$. This can be illustrated by our calculation presented in the Paper II: we compare transmission of the cumulene molecule stretched between (4,4)CNT electrodes. For the two different widths of the gap between the electrodes, the density

of $p_{m=1}$ and $p_{m=-1}$ states along the molecule calculated with DFT method are presented in the Fig. 3.7. The density of states correlates well with the $T(E)$ map since the molecule (carbon wire) is directly coupled to the carbon nanotube. Molecular states with $p_{m=1}$ and $p_{m=-1}$ symmetry correspond to the two conducting channels in the shorter junction. In the longer junction, one of the C-C bonds breaks, and the density distribution changes for $p_{m=-1}$ states, effectively opening a wide gap in this channel and charging the molecule with $\approx$0.1e. We note that slight mismatching of the energies and width of the states and transmission resonances is due to the further adjusted charge of the system in NEGF calculation with open boundary conditions as compared to the neutral state of the system in DFT calculation of projected DOS.

3.4 Conclusion

In this chapter, the quantum transport theories have been introduced, i.e. Landauer theory and non-equilibrium Green's function (NEGF) approach. The NEGF approach can be reduced to the Landauer formalism in the limit of coherent transport regime. The system is divided into three regions: a left lead, a right lead and a central region. To apply the NEGF formalism, it is necessary to calculate the Hamiltonian of lead-molecule-lead to obtain the single-particle Green functions; consequently, DFT is combined in the self-consistent NEGF+DFT approach. Currently, the NEGF+DFT becomes a powerful and rigorous approach, providing quantitative agreement with experiments in many cases. By using this method, we can self-consistently calculate the charge density in the open systems, leading to the transmission coefficients and current voltage characteristics. In the following chapter, the NEGF+DFT approach has been employed to investigate the electron transport properties of various molecular electronic devices.

4. **Summary of papers**

This chapter presents the most significant results included in the thesis. Different types of molecular electronics devices studied in this thesis are classified into three groups: cumulene molecular wires (Paper I, II), a molecular switch based on H-tautomerizaton in phtalocyanine (Paper III) and DNA sequencing in a graphene nanogap (Paper IV, V). All papers employed a combination of density functional theory (DFT) and non-equilibrium Green's functions (NEGF) to perform first principles studies of electron transport.

4.1 Cumulene molecular wires

The carbon wire with double bonds between neighboring atoms is known as a cumulene ($\cdots$ C=C=C=C $\cdots$), while that with alternating single and triple bonds is known as a polyyne ($\cdots$ C$\equiv$C$-$C$\equiv$C $\cdots$). Delocalized bond structure facilitates electron transport through these molecules. The alternating between single and multiple carbon bonds provides the rigid backbone. The polyyne is slightly more stable than the cumulene for straight chain segments [78]. Remarkably, the number of carbon atom in cumulene wires can affect the orientation of the substituents at the ends of the molecule as well as the bond lengths [79, 80]. As a result, the electronic structures and transport properties of cumulene wires depend on whether the number of atoms in the wire is odd or even.

A molecular wire can be one of the major components of nanoelectronic circuits; it is a one-dimensional molecule conducting electrical current between two points. At present, a conjugated molecule conducting electrons via their conjugated-π systems has now become the most promising candidate. The cumulene wire was proposed as the ideal molecular wire [81], predicted to be highly conducting. Subsequent works investigated the transport properties of cumulene wires directly connected to jellium [82, 83] or atomically structured electrodes via carbon double bonds [48, 84]. However, the transport properties of cumulenes using a realistic molecule-lead interface model have not been studied.

In this thesis, first-principles calculations of electron transport were carried out on the cumulene wire using a realistic molecule-lead interface model. Two types of leads are considered; (i) gold, (ii) carbon nanotube, presented in Paper I and Paper II, respectively.

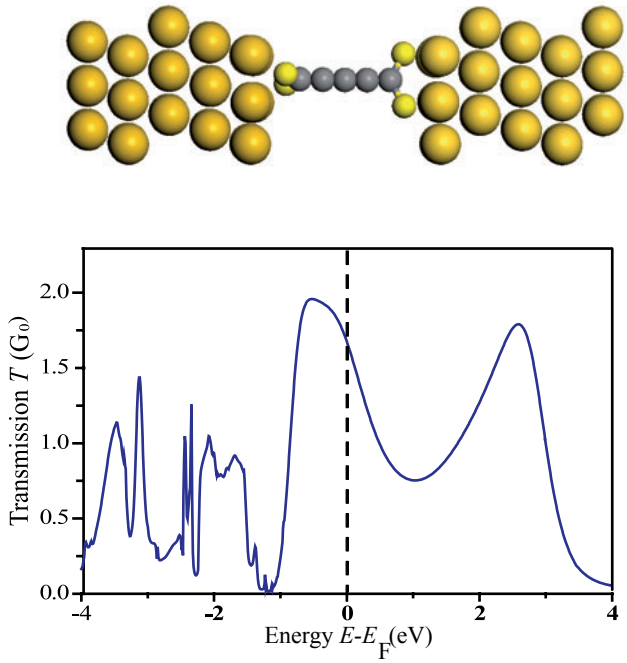

Figure 4.1: The two-probe system for measuring the conductance and IVC of Au(111):S2-cumulene-S2:Au(111) molecular wire junctions (top). Transmission spectra of pentane at zero bias. The broad transmission peak just below the Fermi level corresponds to the lowest unoccupied molecular orbital (bottom).

4.1.1 Paper I

In Paper I, the transport properties of Au(111):S_2-cumulene-S_2:Au(111) molecular wire junctions have been investigated (see Fig. 4.1). We have compared our results with the previous work, which reported the transport properties of the polyyne wires chemisorbed onto gold electrodes [85]. The conductance values of the polyyne wires decreases slowly with wire lengths, whereas those of cumulenes wires vary in an oscillatory manner with the odd-even number of carbon atoms (see Fig. 4.2). The oscillatory conductance of cumulenes has been already explained in the case of jellium electrode [82] by using different occupation of molecular orbitals. For our studied system, however, we have a strong bond between sulphur atoms and Au surfaces, which significantly affected the molecular-level alignments. The oscillatory behavior has been explained by analyzing the transmission eigenstates, contributing to the conductance. The electronic structure is visualized through images of molecular orbitals, explaining the reason for having oscillatory conductance of cumulene wires attached to gold leads via thiol links.

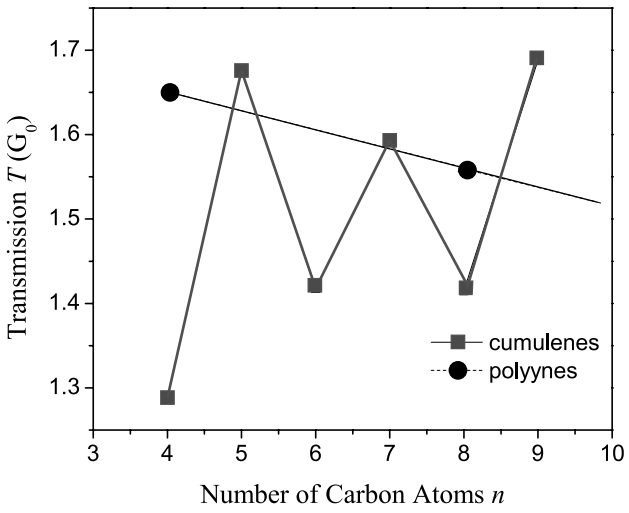

Figure 4.2: Zero-bias transmission $T(E=0,n)$ through the carbon chains.

For odd-n cumulenes (n=5-9), the conductance values are very high and do not show any pronounced dependence on the molecular length, which is a clear signature of ballistic conductance. We show that the high conductance is due to the high density of states in broad lowest unoccupied molecular orbital (LUMO) levels spanning the Fermi level of the electrodes (see Fig.4.1). The conductance, however, is slightly reduced by the effect of backscattering at the contact region.

Over a bias region of ± 1 V, the current-voltage characteristics (IVC) of the cumulene wire is nearly linear, which is a useful property for the 1D molecular wire in nanoelectronic applications. Among all conjugated oligomers, the conductance values of odd-numbered cumulene wires reported so far are the highest. Albeit theoretical results suggest high conductance properties of cumulene wires, research on cumulene wires is still in the early stage due to a problem of stability, especially for the long wire.

4.1.2 Paper II

A new way of producing stable and rigid cumulene wires has been suggested in recent experiments [86, 87]. By using electron irradiation inside a high resolution transmission electron microscope (TEM), a monoatomic carbon wire bridging carbon nanotubes (CNTs) and graphene sheets has been formed, which are more stable and longer than that observed in previous methods [88]. In particular, the cumulene-graphene junction has attracted considerable attention in view of their applications; the formation and breaking of carbon wire bridging the graphene gap has exhibited switching behavior. This switch is very robust; many thousands of cycles were operated without degradation

Figure 4.3: The illustration of C_5 wire bridging between zigzag (4,0)CNTs. The gap width is varied by compressing/stretching junction. By twisting the nanotube, we can change bridging sites and bonding at the junction. The linear carbon wire can transform into either cumulene or polyyne.

[89]. Many subsequent theoretical studies have been carried out for carbon wire-graphene junctions, revealing various types of molecular devices such as molecular switches [90], molecular rectifiers [91], and molecular spintronics [92].

In paper II, we propose a theoretical model of molecular switches based on compressing and stretching of the carbon wire-CNT junction. We have investigated the conductance of cumulenes suspended between the CNTs and graphene sheets (represented by CNTs with infinite radii), and corresponding conductance variation upon stretching. Since the nanotubes with very small radii were observed before breaking of the junction, we have considered the small-diameter tubes; zigzag (4,0)CNT and armchair (4,4)CNT. Varying the gap width between CNT leads results in the change of contact geometries and carbon wire structures, which can transform into either cumulene or polyyne.

We find that the electron transport is significantly affected by the choice of chirality; zigzag or armchair (see Fig.4.4). For the zigzag junction, the distinguishable ON and OFF states (high and low conductance states) are observed, corresponding to the cumulene and polyyne structure, respectively. However, for the armchair junction, there is not enough difference between the ON- and OFF-state to perform switching. The difference in detailed transport behavior of both junctions is due to their entirely different electronic structures and bonding geometries.

We also consider large (infinite) radii of CNTs, represented by the graphene leads. Because of the semiconducting lead for zigzag graphene junction, there is no zero-bias conductance observed, in which the current will be obtained at high bias. For the armchair graphene lead, the conductance values are not much affected by changing of the wire structure.

In the experiment, there is a possibility that the carbon wire can jump to other sites. We therefore investigate how the conductance is affected by the bonding site at the junction for the C_5-wire connected to (4,0)CNT leads (see Fig. 4.3). The range of variation in conductance of the cumulene wires is $\sim 0.2G_0$–$1G_0$, revealing a potential to modulate the conductance. The observed variation is explained by the PDOS analysis of p-orbital components of the cumulene wire. We show that the change of PDOS alignment for the p_x -

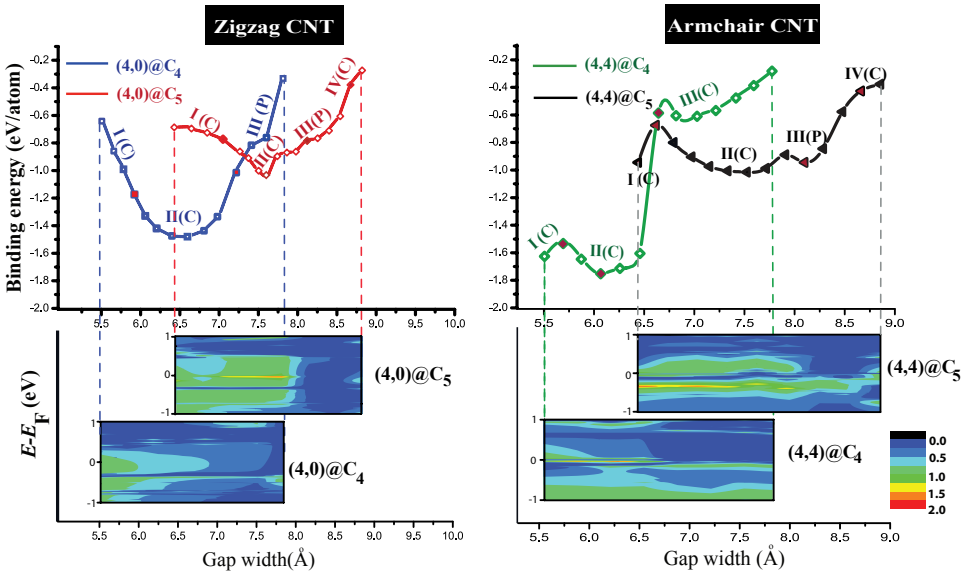

Figure 4.4: Binding energies vs gap width of the C_4- and C_5- wire connected to the (4,0)CNT (left panel) and (4,4)CNT (right panel), and corresponding zero-bias transmission on the energy-length plane T(E=0, L) (bottom). The location of a transition state of structures is marked by red dots (shown in the upper panel). The length-dependent transmission is correlated with the binding energies and wire structures.

and p_y-orbitals results in the change of the number of transmission channels around the Fermi level.

As discussed above, we observe a possibility to operate the molecular switching device by compressing/stretching the carbon wire-zigzag (4,0)CNT junction. To confirm these results, we calculate the IVC of $C_{4,5}$-zigzag CNT junctions, where the C_4 and C_5 wires have different structures depending upon the distance between leads. At bias voltage of 0.2 V, the current ON/OFF ratio of (4,0)@C_4 and (4,0)@C_5 takes the value of $\sim$ 7 and 13, respectively. Based on these results, we can infer that the odd-carbon wire connected to the zigzag CNTs will exhibit switching features by stretching junction without wire breakage.

4.2 A molecular switch based on H-tautomerization in a phthalocyanine

A phthalocyanine molecule is flat and has two hydrogen atoms placed in the inner cavity. The change of the hydrogen atom position in the cavity from horizontal to vertical orientation is commonly known as tautomerization. Such a reaction has significant effects on the electronic structure and transport prop-

erties of the molecule without changing the chemical composition and the molecular frame. These characteristics are expected to be useful for functional devices in molecular electronics. Recently, Liljeroth *et al.* [93] has proposed a new type of molecular switch, induced by the tautomerization reaction of metal-free naphthalocyanine. Note that naphthalocyanine is a derivative of phthalocyanine. Using a low-temperature STM, a voltage pulse at the STM tip can induce a change in the orientation of the hydrogen atom-pair at the center of naphthalocyanine, leading to switching between low and high conductance. Most of switchable molecules involve the effect of the change in molecular conformation; this might not compatible with the aim of controlling molecular electronic circuits. The molecular switch of napthalocyanine molecules is reversible without changing the molecular frame; therefore, it can be integrated in the circuit, which is very beneficial for complex molecular devices.

4.2.1 Paper III

In Paper III, we study the planar electrical transport properties of two hydrogen tautomer configurations of a phthalocyanine (H_2Pc) molecule connected to semi-infinite cumulene and gold leads. The setup with gold leads is inspired by STM experiments in which the molecule is immobilized on a substrate surface and connected to short gold wires in a planar configuration [94]. The transport properties are investigated as a function of the electronic structure of the tautomer state of the molecule, the type of leads, and the coupling between electrodes and the molecule.

Our results show that switching the orientation of the H-H atom pair in the H_2Pc cavity can significantly change the conductance of the molecule, effectively leading to ON and OFF states for both cumulene (Fig. 4.5) and gold (Fig. 4.7) leads. The large change in current, especially in the low-bias regime, is produced by switching the order of nearly degenerate HOMO and HOMO-1 orbitals (see Fig. 4.6). The Fano shapes characterizing the transmission peak close to the Fermi level suggest the two-channel interference between HOMO and HOMO-1 states, leading to two conductance states (“ON” and “OFF”). Furthermore, we show that the potential drop can shift from one metal-molecule contact to the other at intermediate bias, leading to pronounced features in the IVC. On the whole, the underlying reasons for the ON/OFF IVCs in the studied configurations are the presence of two interacting, interfering conduction channels around the Fermi level, being controlled by the tautomer switch.

The junctions with gold leads show negative differential resistance (NDR) at high bias voltage, as well as examples of weak NDR at intermediate bias. NDR is a property of electrical circuits; the current decreases with increasing bias voltage, which can be used for building bi-stable devices and highly functional components like latches, oscillators, memories [95, 96] and logic XOR

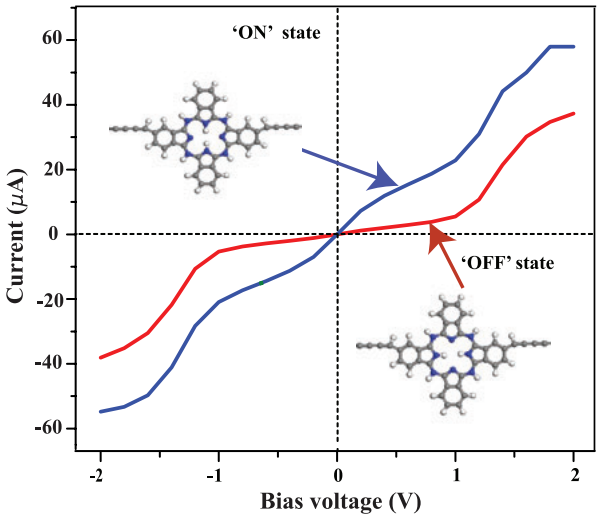

Figure 4.5: The calculated *I-V* characteristics of cumulene(E_F+eV/2)-H_2Pc-cumulene(E_F-eV/2) junctions for two cases of inner hydrogen H-H pair orientation in H_2Pc, obtained in the bias region from -2 to 2 V.

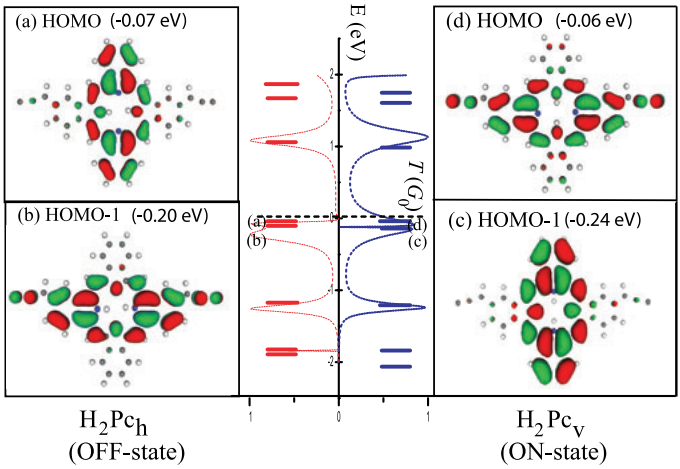

Figure 4.6: The transmission spectra, the MPSH eigenvalues and the MPSH eigenstates around Fermi level of the 'OFF' and 'ON' configurations of cumulene-H_2Pc-cumulene.

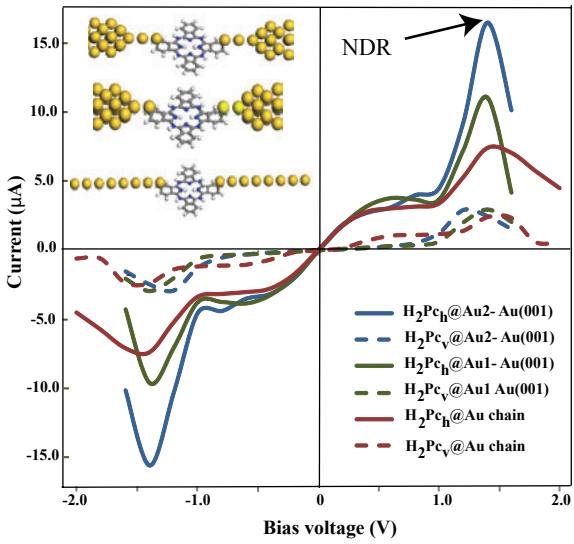

Figure 4.7: I-V characteristics for three cases of Au-H_2Pc-Au junctions for two different H-H pair orientation.

gates [96–98]. Interestingly, the origin of NDR behavior in molecular electronics devices could involve different mechanisms [99–101]. For our studied systems, the reason is the reduced coupling between the molecule and Au lead; thus, the intensity of transmission peaks decrease at high bias voltage, resulting in NDR.

The switching behavior, together with NDR effect, makes H_2Pc an interesting candidate for a multifunctional molecular component. However, we realize that our model system with the two closely space gold contacts is difficult to create in experiment. One possibility to wire circuits could be to first deposit the molecule and then grow the wire. This case has recently been suggested by Okawa *et al.* [102] that demonstrate how to connect single molecules with conductive nanowires.

4.3 DNA sequencing in a graphene nanogap

The fabrication of solid-state nanopores along with their envisioned application for rapid whole-genome sequencing is becoming increasingly sophisticated. However, many extremely challenging questions remain unanswered, especially how to achieve single-base resolution during polynucleotide translocation through the nanopore. To address this issue, it was proposed in early 2010 to employ graphene electrodes, which are atomically thin and thus ideally suited for coupling to one nucleobase at a time [103]. In the middle of 2010, three research groups independently

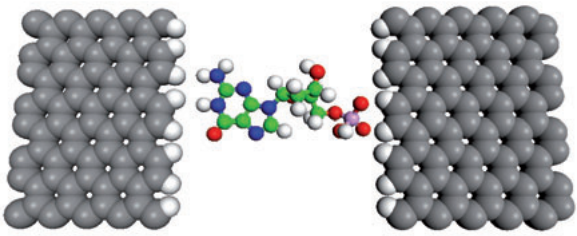

Figure 4.8: The illustration of the double-functionalized two-probe system for measuring the conductance of four target nucleotides. The graphene electrodes are functionalized by a guanidinium ion on the right side and a reader-nucleotide (in the form of cytosine) on the left side.

succeeded in demonstrating the translocation of DNA through graphene nanopores [104–106]

In this thesis, we have theoretically evaluated the potential performance of such a graphene-based DNA sequencing device. The transport properties of the four different nucleotides is influenced by the different base types and orientations of the base with respect to the graphene electrodes (in Paper IV). Furthermore, we have considered the effect of functionalization of the graphene edges that can couple to the nucleotides to improve the sequencing process (in Paper V).

4.3.1 Paper IV

In paper IV, we study the tunneling transport properties of the four nucleotides deoxyadenosine monophosphate (dAMP), deoxythymidine monophosphate (dTMP), deoxyguanosine monophosphate (dGMP), and deoxycytidine monophosphate (dCMP) when located between graphene electrodes with armchair edges chemically passivated by hydrogen (see Fig. 4.8) . Nucleotides can be separated into two groups: purine bases (dGMP, dAMP) and pyrimidine bases (dCMP, dTMP), in which the sizes of the former are larger than that of the latter. As a result, we can easily distinguish electrically between these two cases; the conductance of the dGMP and dAMP is always higher than that of the latter case, resulting from the reduced tunnelling distance.

Variations in the setup included different orientations and positions of the nucleotides relative to the graphene edges, as they would naturally occur during the translocation of DNA. These rotations and lateral shifts were found to have a dramatic effect on the transmission function (see Fig. 4.9). The magnitude of the currents is seen to be ordered in the following hierarchy: $I_{\mathrm{dGMP}} > I_{\mathrm{dAMP}} > I_{\mathrm{dCMP}} > I_{\mathrm{dTMP}}$ (see Fig. 4.10). The large fluctuations in the current are caused by the large variation of nucleotide–graphene coupling

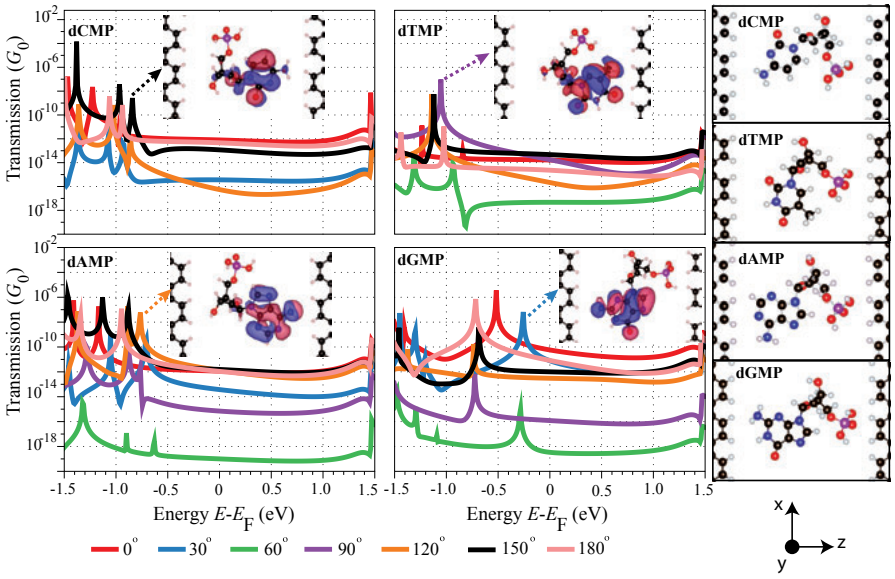

Figure 4.9: The four central panels show the zero-bias transmission function plotted on a semi-logarithmic scale for the four nucleotides, dCMP, dTMP, dAMP, and dGMP. The respective colors of the transmission curves indicate the angle by which the nucleotide has been rotated in a counterclockwise direction around the y-axis as per the legend at the bottom. The insets show isosurface plots of the molecular orbitals responsible for those transmission peaks marked by an arrow. The four vertically arranged panels to the right display the nucleotide orientations corresponding to 0°.

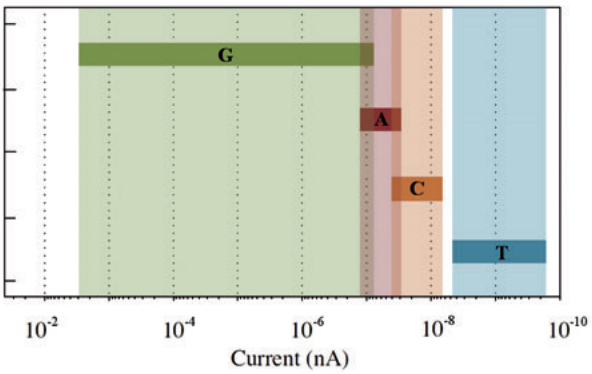

Figure 4.10: Current variation due to nucleotide rotation about the y-axis and translation along the z-axis at a bias of 1 V.

strength. As seen in the Fig. 4.9, we find that dGMP can be distinguished from the other nucleotides due to its strong broad current signal which results from the Fermi energy of the graphene electrodes being close to the wide HOMO peak of dGMP. The other three nucleotides (dAMP, dCMP, and dTMP), which possess HOMO peaks further away from the graphene electrodes Fermi energy, exhibit different characteristic current magnitudes, showing rather little overlap with each other.

Our findings reveal that it should be in principle possible to distinguish between all for nucleotides in the graphene nanogaps setup, which might encourage experimental consideration of this proposed design and take the challenging task of fabricating transverse graphene electrodes in a nanopore setup.

4.3.2 Paper V

With the aim of improving graphene-based DNA sequencing, in paper V, we have explored the effects of functionalizing graphene edges. This setup improves the electronic coupling between electrodes and nucleotides; moreover, it can also lead to a preferred orientation of the target nucleotides relative to the electrodes. With less orientational fluctuations during the translocation process, the associated variance in the tunnelling current signals is reduced. Moreover, it can slow down the translocation speed of the DNA, allowing more time for each individual measurement. In our study, the armchair-edge graphene is functionalized by a guanidinium grabbing phosphate group on one side and a cytosine on the other side (see Fig.4.11).

Our proposed setup shows a capability for sequencing nucleotides in which the current signal of different bases differs by at least 1 order of magnitude. By considering the IVC (see the left panel of Fig. 4.12), two measurements at low and high bias voltages are needed for proper base distinction. For the low bias range ($V_b < 0.4$ V), we can distinguish dGMP and dAMP from other nucleotides based on their current signature. For high bias ($V_b > 0.5$ V), we can distinguish dTMP from dCMP; a low current would indicate the presence of dCMP, whereas a high current would lead to the identification of dTMP. We demonstrate that the motion of transmission resonance peaks under applied bias depends on the electronic structure of each nucleotide and on the coupling of the molecular states of the target nucleotides to the functionalized graphene edges.

Only for dGMP, we observe a negative differential resistance (NDR) effect. The reason of occurrence of NDR is due to the asymmetric HOMO of dGMP and some guanidinium states near the Fermi level through which electrons can tunnel.

Furthermore, the normalized differential conductance, $(dI/dV)/(I/V)$ (see the right panel of Fig. 4.12), has also been considered, offering an even simpler pathway for an unambiguous distinction between all four nucleotides. As it can be seen from the right panel of 4.12, dTMP can be distinguished at about

0.45 V by an exceptionally high $(dI/dV)/(I/V)$ value. Also, dGMP can be uniquely identified at 0.50 V by the unusual negative value of dI/dV. The other two nucleotides show either moderate dI/dV values (dAMP) or virtually zero dI/dV (dCMP), leading to their respective distinction.

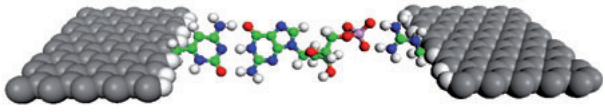

Figure 4.11: Illustration of the double-functionalized two-probe system for measuring the conductance of target nucleotides. The graphene electrodes are functionalized by a guanidinium ion on the right side and a reader-nucleobase (in the form of cytosine) on the left side. The target nucleotide shown here is dGMP.

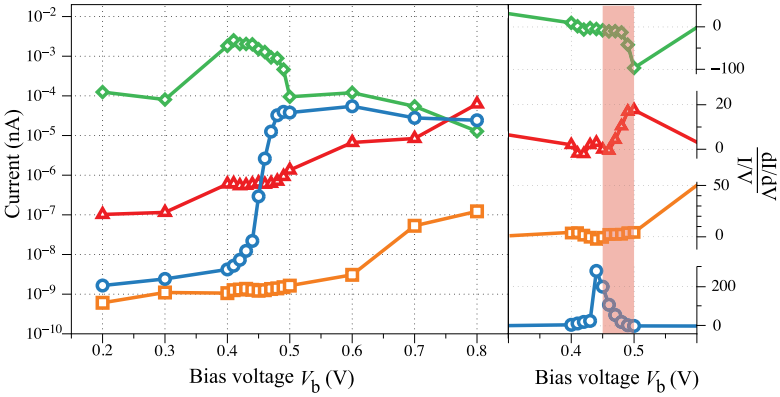

Figure 4.12: The current-voltage curves plotted on a semi-logarithmic scale in the left panel for the four target nucleotides: dGMP (green diamonds), dAMP (red triangles), dCMP (orange squares), and dTMP (blue circles). In the right panel, the normalized first derivative of tunneling current, $(dI/dV)/(I/V)$, showing a possibility for distinguishing the four nucleotides with a single voltage scan.

5. Summary

Electron transport through a single molecule or an atomic-size material is a sophisticated quantum scattering process. With advancements in experimental techniques, it is now possible to make contacts to single molecules to investigate their properties as molecular electronic devices. From a computational point of view, understanding the transport phenomena in such devices would enable us to explain experimental results and develop new molecular devices with functionality suitable for practical applications.

This thesis focuses on electronic and transport properties of molecular electronic devices. We have used the non-equilibrium Green's function method (NEGF) combined with density functional theory (DFT), providing first principle transport modelling for molecular electronics. By using the NEGF-DFT approach, we can describe the electrical conduction properties of nanoscale systems at an atomistic level. In addition, the DFT also allows us to describe the electronic structure of the whole system, including the molecule and the surface of the contacting electrodes. Systems containing up to few hundred atoms can currently be studied at the atomic-level of detail.

A number of applications for the molecular electronics devices have been described. The first class of studied systems concerns the functionality of a conducting molecular connector. We study cumulene molecular wires showing ballistic transport in molecular devices. Two types of junction have been considered: cumulene wire sandwiched between two gold electrodes via thiolate bonds Au(111):S_2-cumulene-S_2:Au(111); and cumulene suspended between two carbon nanotubes. For the gold leads, we find that the cumulene shows the capability as 1-D molecular metallic wires due to very high conductance and nearly linear IVC in the low bias regime. Unfortunately, in the experiment, a cumulene wire using a realistic molecule-lead interface model is difficult to fabricate due to the problem with stabilization of the wire. However, it was recently suggested that cumulene wires bridging CNTs could be produced in the experiment, which are extremely robust and easy to fabricate by stretching the nanotube up to the breaking point. We have therefore studied the transport properties of carbon wires suspended between zigzag and armchair CNTs, and studied corresponding conductance variation upon stretching. The characteristics of a molecular switch operated by compressing/stretching is observed in the case of the zigzag junction. Moreover, we suggest a way to modulate the conductance with changing bridging sites and bonding at the junction by twisting the nanotube.

Introducing the switching functionality into molecular wire is one of the ways towards the practical application of the molecular electronics devices. We considered molecular junction with two possible H-tautomer configurations of phthalocyanine (H_2Pc). As known from a series of STM experiments, hydrogen tautomerization in the H_2Pc is the reversible switching process induced under increased applied bias. We therefore investigate the switching based on the H-tautomerization in H_2Pc laterally connected to gold and cumulene leads. In this configuration, electrical current is running along H_2Pc's molecular plain, while in STM study the current is running across the plain. The prominent difference in molecular conductance between the ON and OFF switched states (different orientations of the H-H pair) is demonstrated, especially in the low bias regime. The reason for the large change in the current is that the current transport proceeds via two interfering channels involving two highest occupied molecular orbitals close to the Fermi level. Hydrogen tautomerization affects the electronic state of H_2Pc by switching the orbital character of these orbitals, dramatically influencing the interference effect and the positions and shapes of the transmission amplitude around the Fermi level.

As an important application of the molecular electronics, we consider molecular sensors. There has been developed a potential molecular electronics approach for rapid genome sequencing - reading out the order of nucleobases in a ssDNA molecule by pulling it between a pair of nanoscale electrodes and reading out the transverse current through each base. In particular, its potential for single-base resolution offers unparalleled advantages. However, the practical realisation of the method is hindered by the need to fabricate electrodes that are comparable in thickness to a single DNA unit - nucleotide. We have characterized a graphene-based DNA sequencing device that can achieve the required sensitivity to electrically distinguish between the four types of nucleobases in DNA. Graphene electrodes are the natural choice for the problem because graphene is conductive yet atomically thin material. Furthermore, we consider the effect of functionalization of the graphene edges with the molecules that can couple to the nucleotides to enhance the sequencing process.

Overall, we have obtained and presented the results from the state of art of *ab initio* simulations, providing insight to electron transport processes at the atomic scale. It would be very interesting to continue exploring the transport properties of such setups following the development of the modern nanoscale technology in the future.

6. **Acknowledgements**

I am deeply indebted to so many people that it is somewhat unlikely to express my sincere gratitude to all of them. Without their kindest assistance and encouragement, this thesis could not have been achieved.

First and foremost, I would humbly like to thank my supervisor Prof. Rajeev Ahuja, who gave me the opportunity to do my PhD study at the Condensed Matter Theory Group, Department of Physics & Astronomy at Uppsala University. I am most grateful to him for his patience, encouragement, and invaluable support throughout my study. Also, I would like to acknowledge the Royal Thai Government for financial support on my study in Sweden.

My special thanks go to Anton Grigoriev, for being a great mentor throughout my PhD study, for useful suggestions, thought-provoking discussions and revision of all my papers and the thesis. Thank you very much to Prof. Göran Wendin for his greatest help and continuous guidance as well as for a fruitful collaboration. My grateful expression also goes to Ralph H. Scheicher for introducing me to the DNA sequencing project, for the productive collaboration and for being so kind whenever I need his comments and suggestions. I am also very grateful to other collaborators; Biswarup, Rikard E. and others.

Besides, I would like to acknowledge the Uppsala University Uni-Molecular Electronic Center (U3MEC), for providing a wonderful working environment as well as sharing the knowledge within the field of molecular electronics. Of course, Henrik Ottosson, who is the coordinator of U3MEC, is especially thanked for all his ideas, comments and open discussion.

During my PhD study, several special thanks must be mentioned here with pleasure and gratitude to some current and former members of our group; to Pornjuk for invaluable friendship and greatest support whenever I needed; to Henrik L. for translating the summary of the thesis into Swedish; to Moyses for hospitality and very good dinners; to Peter L. for kind suggestions when I encountered problems in compiling codes; to Duck Young for Gim-Bahp and Korean instant noodles; to Pooja, Diana, Johan, Karel and Younsuk for such enjoyable time playing badminton together. Cordially thanks also go to my lovely friends: Love, Cecilia, Anden, Fedrik, Wei, Zhimei and others.

Although I have been away from my home for such a long time, I have never really felt lonely in Uppsala. I would like to thank all friends for making my life here pleasant and worthwhile. First, I simply have no words that can adequately express my most gratitude to P Jeab, P Joy, P Jum, P Juk and

P Jate. Thank you so much for all your 24-hour help, encouragement and meaningful friendship. Further thanks go to P Ping for your delicious menus and introducing me to the world of bioinformatik; to Siri for happy lunchtime during my last PhD year; to Anders O. and Gunnar P. for great time together; to P Mee for a nice cover of this thesis. I am also very grateful to R Slil, R Tassanee, P Jang, P On, P Taw, N Pom, P Noy, P Tuk for your kindness and super delicious Thai food. I wish to thank all Thai students in Uppsala for being such great friends: Aom, Coam, Noinar, P Nok, M, Fiat, Alin, Jub, P Chai, Nit, Grace, Wow, Air, SomO and others.

Last, but not least, I would like to wholeheartedly thank my family for their greatest love, consistent support and endless encouragement. I could never have come this far without you.

7. Sammanfattning på Svenska

Material kan byta skepnad när de blir nanometerstora. För att få snabbare datorer har datortillverkarna krympt komponenterna på datorchipen så att storleken nu kan räknas i nanometer. Men nu känner de av den magiska nanogränsen. Till exempel börjar elektronerna att smita genom de strömförande ledningarnas väggar. Det kallas för att elektronen tunnlar, vilket de inte får göra i någon större utsträckning om en dator ska fungera. Tanken med nanoteknik är att utnyttja nanovärldens lagar istället för att kämpa emot dem.

Elektron transport genom en enda molekyl eller genom ett material på atomnivå är en sofistikerad process som måste beskrivas med hjälp av kvantmekanisk spridning. Framsteg inom olika experimentella tekniker, har lett till att det nu är möjligt att skapa kontakter till enstaka molekyler för att undersöka deras egenskaper och om de kan användas som elektriska komponenter. För att kunna förklara de experimentellt uppmätta resultaten, och för att förutse vilka molekyler som skulle kunna fungera som komponenter behövs en bra teoretisk förståelse av dessa transportegenskaper. I denna avhandling har vi undersökt dessa egenskaper med hjälp av kvantmekaniska beräkningar baserade på täthetsfunktionalteori och icke-jämvikts Greensfunktioner.

För männskligheten är det nytt och revolutionerade att kunna bygga med enstaka atomer, men för naturen är det inget nytt. Ungefär som klämmor på en elkabel kan man koppla DNA-molekyler mot varandra på en bestämd plats. Elektroner kan sedan hoppa längs DNA-molekylen, men det är svårt att leda elströmmen längs den. Vi utforskar istället möjligheterna att använda andra molekyler som en riktig nanokabel, en s.k. nanoledning.

För att bygga dessa nanokablar kan man använda "cumulene" molekyler (kol-trådar). Två typer av enheter har undersökts: cumulene sammankopplade med två guld elektroder via en guld-svavel bindning och cumulene svävande mellan två kolnanorör. För guld-kol-ledningarna, kan vi se att cumulene kan fungera som en molekylär kabel med metalliska egenskaper, vilket innebär att den har mycket hög konduktans (ledningsförmåga) och nästan linjärt beroende mellan ström och spänning för låga spänningar. Tyvärr så har experiment visat att det är väldigt svårt att tillverka en cumulene-tråd som är stabil under de här förhålanderna . Däremot verkar det som att det går att tillverka stabila cumelene-trådar mellan kolnanorör, genom att sträcka ut kolnanoröret till bristningsgränsen. Vi har därför även studerat transport egenskaperna av

dessa kol-trådar svävande mellan kolnanorör och även hur ledningsförmågan påverkades av utsträckningen av kolnanoröret. Beroende på vilken typ av kolnanorör som används kan vi observera att tråden fungerar som en molekylär brytare när man drar ut eller trycker ihop den. Dessutom visar vi att det går att ändra konduktansen genom att vrida på kolnanoröret och därmed ändra kontaktplatsen mellan tråd och rör.

För att kunna bygga användbara elektriska komponenter av molekylära enheter är något som fungerar som en brytare väldigt viktigt. Vi har därför studerat två möjliga väte-tautomerer (två skilda strukturer som står i snabb jämvikt med varandra dock oftast svåra att isolera separat) i ftalocyanin-molekylen (H_2Pc). När vi ansluter vår H_2Pc till antingen guld- eller cumulene-kontakter kommer den elektriska strömmen att ledas längs molekylens plan och vi kan se stora skillnader mellan "PÅ" och "AV" lägen (olika orienteringar av väte-väte bindningen i molekylen). Vi kan även visa att denna skillnad beror på skillnader i vilka elektron-orbitaler som medverkar i elektrontransporten.

En annan viktig tillämpning där molekylär elektronik kan komma att spela en viktig roll är som sensorer. Här visar vi upp en metod som använder molekylär elektronik för snabb genom-sekvensering. Detta görs genom att dra DNA-spiralen mellan två nanoelektroder och läsa nukleobaserna en efter en via en ström genom den, karakteristisk för varje bas. Det finns fortfarande problem att realisera den här metoden praktiskt, framförallt eftersom man behöver elektroder av samma tjocklek som en nukleotid (en DNA-enhet). Vi har därför här valt att jobba med grafen elektroder, vilket kan ses som ett naturligt val eftersom dels leder grafen ström mycket bra men framförallt är det endast ett atomlager tjockt. Detta medför att det är möjligt att få en tillräckligt känslig uppställning för att särskilja de enskilda DNA-baserna. Vi har även utforskat om man kan öka känsligheten i uppställningen genom att koppla andra molekyler till grafen-elektroderna.

Sammanfattningsvis har vi presenterat resultat från det allra senaste inom *ab initio* (från första principer) beräkningar som ger inblick i hur elektrontransport processer sker på atomär skala. Det finns en enorm potential att på längre sikt delvis ersätta traditionell elektronik baserad på kisel med molekylär elektronik. Det innefattar även ny utrustning för medicinsk diagonstik, ny utrustning för miljöprover samt nya typer av sensorer. Framförallt, att få möjligheten att studera så små prover som enskilda molekyler öppnar fantastiska möjligheter både för forskningen men även för vardagslivet. Det skulle vara mycket intressant att fortsätta med undersökningar av transportegenskaper av liknande uppställningar och följa utvecklingen av den moderna nanotekniken in i framtiden.

Bibliography

[1] G. E. Moore. *Electronics Magazine*, 38, 1965.

[2] K. Bernstein, D. J. Frank, A. E. Gattiker, W. Haensch, B. L. Ji, S. R. Nassif, E. J. Nowak, D. J. Pearson, and N. J. Rohrer. High-Performance CMOS Variability in the 65-nm Regime and Beyond. *IBM J. Res. Dev.*, 50:433–449, 2006.

[3] Y. Wang, U. Bhattacharya, F. Hamzaoglu, P. Kolar, Yong-Gee Ng, L. Wei, Y. Zhang, K. Zhang, and M. Bohr. A 4.0 GHz 291 Mb Voltage-Scalable SRAM Design in a 32 nm High-k + Metal-Gate CMOS Technology with Integrated Power Management. *IEEE J. Solid-St. Circ.*, 45:103–110, 2010.

[4] S. Saxena, C. Hess, H. Karbasi, S. Tonello A. Rossoni, P. McNamara, S. Lucherini, S. Minehane, C. Dolainsky, and M. Quarantelli. Variation in Transistor Performance and Leakage in Nanometer-Scale Technologies. *IEEE T. on Electron Dev.*, 55:131–144, 2008.

[5] B. H. Calhoun, Y. Cao, X. Li, K. Mai, L.T. Pileggi, R. A. Rutenbar, and K. L. Shepard. Digital Circuit Design Challenges and Opportunities in the Era of Nanoscale CMOS. *Proc. IEEE*, 96:343–365, 2008.

[6] T. W. Ebbesen, H. J. Lezec, H. Hiura, J. W. Bennett, H. F. Ghaemi, and T. Thio. Electrical Conductivity of Individual Carbon Nanotubes. *Nature*, 382:54–56, 1996.

[7] M. A. Reed, C. Zhou, C. J. Muller, T. P. Burgin, and J. M. Tour. Conductance of a Molecular Junction. *Science*, 10:252–254, 1997.

[8] L. A. Bumm *et al.* Are Single Molecular Wires Conducting?. *Science*, 271:1705–1707, 1996.

[9] J. Jortner, A. Nitzan, and M. A. Ratner. *Introducing Molecular Electronics, Lecture Notes in Physics Vol. 680*. Springer, Heidelberg, 2005.

[10] R. Martel, T. Schmidt, H. R. Shea, T. Hertel, and Ph. Avouris. Single- and Multi-wall Carbon Nanotube Field-Effect Transistors. *App. Phys. Lett.*, 73:2447–2449, 1998.

[11] H. E. Katz and Z. Bao. The Physical Chemistry of Organic Field-Effect Transistors. *J. Phys. Chem. B*, 104:671–678, 2000.

[12] A. Dehon. Array-Based Architecture for FET-Based, Nanoscale Electronics. *IEEE T. Nano.*, 2:23–32, 2003.

[13] Z. J. Donhauser *et al.* Conductance Switching in Single Molecules Through Conformational Changes. *Science*, 292(5525):2303–2307, 2001.

[14] C. P. Collier *et al.* A [2]Catenane-Based Solid State Electronically Reconfigurable Switch. *Science*, 289(5482):1172–1175, 2000.

[15] Y. Chen, G. Y. Jung, D. A. A Ohlberg, X. Li, D. R. Stewart, J. O. Jeppesen, K. A. Nielsen, J. F. Stoddart, and R. S. Williams. Nanoscale Molecular-switch Crossbar Circuits. *Nanotechnology*, 14(4):462–468, 2003.

[16] A. S. Martin, J. R. Sambles, and G. J. Ashwell. Molecular Rectifier. *Phys. Rev. Lett.*, 70:218–221, 1993.

[17] A. Staykov, D. Nozaki, and K. Yoshizawa. Theoretical Study of Donor-π-Bridge-Acceptor Unimolecular Rectifier. *J. Phys. Chem. C*, 111:11699–11705, 2007.

[18] M. P. Samanta, W. Tian, S. Datta, and JI Henderson. Electronic Conduction through Organic Molecules. *Phys. Rev. B*, 53:R7626–R7629, 1996.

[19] C. Wang, Y. Hu, C. M. Lieber, and S. Sun. Ultrathin Au Nanowires and Their Transport Properties. *J. Am. Chem. Soc.*, 130(28):8902–8903, 2008.

[20] A. Javey, H. Kim, M. Brink, Q. Wang, A. Ural, J. Guo, P. McIntyre, P. McEuen, M. Lundstrom, and H. Dai. High-κ dielectrics for advanced carbon- nanotube transistors and logic gates. *Nat. Mater.*, 1(4):241–246, 2002.

[21] P. A. Smith, C. D. Nordquist, T. N. Jackson, T. S. Mayer, B. R. Martin, J. Mbindyo, and T. E. Mallouk. Electric-field Assisted Assembly and Alignment of Metallic Nanowires. *App. Phys. Lett.*, 77(9):1399–1401, 2000.

[22] D Fichou. Structural Order in Conjugated Oligothiophenes and its Implications on Opto-electronic Devices. *J. Mat. Chem*, 10:571–588, 2000.

[23] T. Rueckes *et al.* Carbon Nanotube-Based Nonvolatile Random Access Memory for Molecular Computing. *Science*, 289:94–97, 2000.

[24] R. Waser and M. Aono. Nanoionics-based Resistive Switching Memories. *Nat. Mater.*, 6:833–840, 2007.

[25] A. Kolmakov and M. Moskovits. Chemical Sensing and Catalysis by One-Dimensional Metal-Oxide Nanostructures. *Annu. Rev. Mater. Res.*, 34:151–180, 2004.

[26] G. Raschke, S. Brogl, A. S. Susha, A. L. Rogach, T. A. Klar, J. Feldmann, B. Fieres, N. Petkov, T. Bein, A. Nichtl, and K. Kürzinger. Gold Nanoshells Improve Single Nanoparticle Molecular Sensors. *Nano Lett.*, 4(10):1853–1857, 2004.

[27] M. C. Petty. *Molecular Electronics: From Principles to Practice*. John Wiley & Sons, Ltd., 2007.

[28] J. R. Health and M. A. Ratner. Molecular electronics. *Physics Today*, 56:43–49, 2003.

[29] A. Aviram and M. A. Ratner. Molecular rectifiers. *Chem. Phys. Lett.*, 29:277–283, 1974.

[30] M. A. Reed, C. Zhou, C. J. Muller, T. P. Burgin, and J. M. Tour. Conductance of a molecular junction. *Science*, 278:252–254, 1997.

[31] J. V. Ruitenbeek, E. Scheer, and B. Weber. *Introducing Molecular Electronics, Lecture Notes in Physics Vol. 680*. Springer, Heidelberg, 2005.

[32] L. Grüter, F. Cheng and T. T. Heikkilä, M. T. González, F. Diederich, C. Schönenberger, and M. Calame. Resonant Tunnelling through a C_60 Molecular Junction in a Liquid Environment. *Nanotechnology*, 16:2143–2148, 2005.

[33] C. A. Martin, D. Ding, H. S. J. V. D. Zant, and J. M. V. Ruitenbeek. Lithographic Mechanical Break Junctions for Single-Molecule Measurements in Vacuum: Possibilities and Limitations. *New J. Phys.*, 10:065008, 2008.

[34] Y. Yang *et al.* Conductance Histogram Evolution of an EC–MCBJ Fabricated Au Atomic Point Contact. *Nanotechnology*, 22:275313, 2011.

[35] H. Park. Molecular electronics: Charges feel the heat. *Nat. Mater.*, 6:330–331, 2007.

[36] H. Park, A. K. L. Lim, A. P. Alivisatos, J. Park, and P. L. McEuen. Fabrication of metallic electrodes with nanometer separation by electromigration. *Appl. Phys. Lett.*, 75:301–303, 1999.

[37] A. F. Morpurgo, C. M. Marcus, and D. B. Robinson. Controlled Fabrication of Metallic Electrodes with Atomic Separation. *Appl. Phys. Lett.*, 74:2084–2086, 1999.

[38] C. Z. Li, H. X. He, and N. J. Tao. Quantized Tunneling Current in the Metallic Nanogaps Formed by Electrodeposition and Etching. *Appl. Phys. Lett.*, 77:3995–3997, 2000.

[39] D. C. Ralph, C. T. Black, and M. Tinkham. Spectroscopic Measurements of Discrete Electronic States in Single Metal Particles. *Phys. Rev. Lett*, 74:3241–3244, 1995.

[40] S. M. Iqbal, G. Balasundaram, S. Ghosh, D. E. Bergstrom, and R. Bashir. Direct Current Electrical Characterization of ds-DNA in Nanogap Junctions. *App. Phys. Lett.*, 86(15):153901–3, 2005.

[41] C. A. Martin, J. M. V. Ruitenbeek, and H. S. J. V. D. Zant. Sandwich-Type Gated Mechanical Break Junctions. *Nanotechnology*, 21:265201, 2010.

[42] C. P. Collier *et al.* Electronically Configurable Molecular-Based Logic Gates. *Science*, 285:391, 1999.

[43] K. I. Ramachandran, G. Deepa, and K. Namboori. *Computational Chemistry and Molecular Modelling: Principles and Applications*. Springer, 2008.

[44] S. Datta. *Electronic Transport in Mesoscopic Systems*. Cambridge University Press, 1995.

[45] H. Haug and A.P. Jauho. *Quantum Kinetics in Transport and Optics of Semiconductors*. Springer-Verlag Berlin, 1996.

[46] J. Taylor, H. Guo, and J. Wang. Ab initio modeling of quantum transport properties of molecular electronic devices. *Phys. Rev. B*, 63:245407–13, 2001.

[47] J. J. Palacios, A. J. Pérez-Jiménez, E. Louis, E. SanFabián, and J.A Vergés. First-Principles Approach to Electrical Transport in Atomic-Scale Nanostructures. *Phys. Rev. B*, 66:035322–14, 2002.

[48] M. Brandbyge, J. L. Mozos, P. Ordejón, J. Taylor, and K. Stokbro. Density-Functional Method for Nonequilibrium Electron Transport. *Phys. Rev. B*, 65:165401–17, 2002.

[49] A. R. Rocha, V. M. Garcia-Saurez, S. W. Bailey, C. J. Lambert, J. Ferrer, and S. Sanvito. Towards molecular spintronics. *Nat. Mater.*, 4:335–339, 2005.

[50] A. W. Ghosh, P. S. Damle, S. Datta, and A. Nitzan. Molecular Electronics: Theory and Device Prospects. *MRS Bulletin*, 29:391–395, 2004.

[51] P. S. Damle, A. W. Ghosh, and S. Datta. *Phys. Rev. B*, 64:R201403, 2001.

[52] R. M. Martin. *Electronic Structure: Basic Theory and Practical Methods*. Cambridge University Press, 2004.

[53] D. S. Sholl and J. A. Steckel. *Density Functional Theory: A Practical Introduction*. A John Wiley & Sons, Inc., 2009.

[54] F. Jensen. *Introduction to Computational Chemistry*. John Wiley & Sons, Ltd., 2007.

[55] W. Kohn, A. D. Becke, and R. G. Parr. Density Functional Theory of Electronic Structure. *J. Phys. Chem*, 100:12974–12980, 1996.

[56] R. G. Parr. Density Functional Theory. *Ann. Rev. Phys .Chem.*, 34:631–656, 1983.

[57] P. Hohenberg and W. Kohn. Inhomogeneous Electron Gas. *Phys. Rev.*, 136:B864–B871, 1964.

[58] W. Kohn and L. J. Sham. Self-Consistent Equations Including Exchange and Correlation Effects. *Phys. Rev.*, 140:A1133–A1138, 1965.

[59] J. P. Perdew and Y. Wang. Accurate and Simple Analytic Representation of the Electron-gas Correlation Energy. *Phys. Rev. B*, 45:13244–13249, 1992.

[60] J. P. Perdew, K. Burke, and M. Ernzerhof. Generalized Gradient Approximation Made Simple. *Phys. Rev. Lett*, 77:3865–3868, 1996.

[61] J. P. Perdew, A. Ruzsinszky, J. Tao, V. N. Staroverov, G. E. Scuseria, and G. I. Csonka. Prescription for the Design and Selection of Density Functional Approximations: More Constraint Satisfaction with Fewer Fits.

[62] Ž. Crljen, P. Lazić, D. Šokčević, and R. Brako. Relaxation and Reconstruction on (111) Surfaces of Au, Pt, and Cu. *Phys. Rev. B*, 68:195411–8, 2003.

[63] P. Ordejón, E. Artacho, and J. M. Soler. Self-Consistent Order-N Density-Functional Calculations for Very Large Systems. *Phys. Rev. B*, 53(16):10441–10444, 1996.

[64] A. R. Rocha, V. M. García-suárez, S. W. Bailey, C. J. Lambert, J. Ferrer, and S. Sanvito. Towards Molecular Spintronics. *Nat. Mater.*, 4(4):335–339, 2005.

[65] A. R. Rocha, V. M. García-Suárez, S. Bailey, C. Lambert, J. Ferrer, and S. Sanvito. Spin and Molecular Electronics in Atomically Generated Orbital Landscapes. *Phys. Rev. B*, 73(8):085414–22, 2006.

[66] C. Kittel. *Introduction to Solid State Physics:* 8^{th} *edition*. John Wiley & Sons, Ltd., 2005.

[67] H. J. Monkhorst and D. J. Pack. On Special Points for Brillouin Zone Integrations. *Phys. Rev. B*, 13:5188–5192, 1976.

[68] D. R. Hamann, M. Schlüter, and C. Chiang. Norm-Conserving Pseudopotentials. *Phys. Rev. Lett*, 43:1494–1497, 1979.

[69] C. Fiolhais, F. Nogueira, and M. Marques. *A Primer in Density Functional Theory*. Springer, 2003.

[70] A. A Katsnelson *et al*. *Computational Methods in Condensed Matter: Electronic Structure*. American Institute of Physics, 1992.

[71] N. Troullier and J. L. Martins. Efficient pseudopotentials for plane-wave calculations. *Phys. Rev. B*.

[72] A. Kolmakov and M. Moskovits. Chemical Sensing and Catalysis by One-Dimensional Dimensional Metal-Oxide Nanostructures. *Annu. Rev. Mater. Res.*, 34:151–180, 2004.

[73] W. Y. Kim, Y. C. Choi, S. K. Min, Y. Cho, and K. S. Kim. Application of Quantum Chemistry to Nanotechnology: Electron and Spin Transport in Molecular Devices. *Chem. Soc. Rev.*, 38:2319–2333, 2009.

[74] M. D. Ventra. *Electrical Transport in Nanoscale Systems*. Cambridge University Press, 2008.

[75] M. Büttiker, Y. Imry, R.Landauer, and S.Pinhas. Generalized Many-Channel Conductance Formula With Application to Small Rings. *Phys. Rev. B*, 31:6207–6215, 1985.

[76] J. C. Cuevas and E. Scheer. *Molecular Electronics: An Introduction to Theory and Experiment*. World Scientific Co. Pte. Ltd., 2010.

[77] M. Paulsson. Non Equilibrium Green's Functions for Dummies: Introduction to the One Particle NEGF equations. *http://arXiv.org/abs/cond-mat/0210519v2*.

[78] M. M. Haley. Carbon allotropes: On the road to carbyne. *Nat. Chem.*, 2:912–3, 2010.

[79] S. Hino, Y. Okada, K. Iwasaki, M. Kijima, and H. Shirakawa. Electronic Structures of Cumulene Type Carbyne Model Compounds: A Typical Example of One-Dimensional Quantum Well. *Chem. Phys. Lett.*, 372:59–65, 2003.

[80] U. Mölder, P. Burk, and I. A. Koppel. Quantum Chemical Calculations of Linear Cumulene Chains. *J. Mol. Struct: (Theochem)*, 712:81–89, 2004.

[81] W. Beck, B. Niemer, and M. Wieser. *Chem., Int. Ed. Engl.*, 32:923, 1993.

[82] N. D. Lang and Ph. Avouris. Oscillatory conductance of carbon-atom wires. *Phys. Rev. Lett.*, 81:3515–3518, 1998.

[83] N. D. Lang and Ph. Avouris. Carbon-Atom Wires: Charge-Transfer Doping,Voltage Drop, and the Effect of Distortions. *Phys. Rev. Lett.*, 84:358–361, 2000.

[84] J. J. Palacios, A. J. Pérez-Jiménez, E. Louis, E. SanFabián, and J. A. Vergéss. First-Principles Approach to Electrical Transport in Atomic-Scale Nanostructures. *Phys. Rev. B*, 66:035322–14, 2002.

[85] Ž. Crljen and G. Baranović. Unusual Conductance of Polyyne-Based Molecular Wires. *Phys. Rev. Lett.*, 98:116801–4, 2007.

[86] H. E. Troiani, M. Miki-Yoshida, G. A. Camacho-Bragado, M. A. L. Marques, A. Rubio, J. A. Ascencio, and M. Jose-Yacaman. Direct Observation of the Mechanical Properties of Single-Walled Carbon Nanotubes and Their Junctions at the Atomic Level. *Nano Letters*, 3:751–755, 2003.

[87] C. Jin, H. Lan, L. Peng, K. Suenaga, and S. Iijima. Deriving Carbon Atomic Chains from Graphene. *Phys. Rev. Lett.*, 102(20):205501–4, 2009.

[88] H. Hopf. *Classical in Hydrocarbon Chemistry*. Wiley-VCH, 2000.

[89] B. Standley, W. Bao, H. Zhang, J. Bruck, C. N. Lau, and M. Bockrath. Graphene-Based Atomic-Scale Switches. *Nano Lett.*, 8:3345–3349, 2008.

[90] E. Erdogan, I. Popov, C. G. Rocha, G. Cuniberti, S. Roche, and G. Seifert. Engineering Carbon Chains from Mechanically Stretched Graphene-Based Materials. *Phys. Rev. B*, 83:041401(R), 2011.

[91] M. Zeng, L. Shen, M. Zhou, C. Zhang, and Y. Feng. Graphene-Based Bipolar Spin Diode and Spin Transistor: Rectification and Amplification of Spin-Polarized Current. *Phys. Rev. B*, 83:115427–6, 2011.

[92] Z. Zanolli, G. Onida, and J-C Charlier. Quantum Spin Transport in Carbon Chains. *ACS nano*, 4:5174–5180, 2010.

[93] P. Liljeroth, J. Repp, and G. Meyer. Current-induced hydrogen tautomerization and conductance switching of naphthalocyanine. *Nature*, 317:1203–1206, 2007.

[94] G. V. Nazin *et al.* Visualization and Spectroscopy of a Metal-Molecule-Metal Bridge. *Science*, 302:77–81, 2003.

[95] M. A. Reed, J. Chen, A. M. Rawlett, D. W. Price, and J. M. Tour. Molecular Random Access Memories. *App. Phys. Lett.*, 78:3735–3737, 2001.

[96] C. P. Husband, S. M. Husband, J. S. Daniels, and J. M. Tour. Logic and Memory with Nanocell Circuits. *IEEE T. on Electron Dev.*, 50:1865–1975, 2003.

[97] J. Sköldberg and G. Wendin. Reconfigurable Logic in Nanoelectronic Switching Networks. *Nanotechnology*, 18:485201, 2007.

[98] J. Sköldberg, C. Önnheim, and G. Wendin. Nanocell Architecture for Configurable Computing with Molecular Electronics. *IEEE Trans. Circuits and Systems I*, 54:2461, 2007.

[99] S. Y. Quek, J. B. Neaton, M. S. Hybertsen, E. Kaxiras, and S. G. Louie. Negative Differential Resistance in Transport through Organic Molecules on Silicon. *Phys. Rev. Lett.*, 98:066807, 2007.

[100] F.J. Ribeiro, W. Lu, and J. Bernholc. Doping-Dependent Negative Differential Resistance in Hybrid Organic/Inorganic Si Porphyrin Si Junctions. *ACS Nano*, 2:1517–1522, 2008.

[101] R. Pati, M. McClain, A. Bandyopadhyay. Origin of Negative Differential Resistance in a Strongly Coupled Single Molecule-Metal Junction Device. *Phys. Rev. Lett.*, 100:246801, 2008.

[102] Y. Okawa, S. K. Mandal, C. Hu, Y. Tateyama, S. Goedecker, S. Tsukamoto, T. Hasegawa, J. K. Gimzewski, and M. Aono. Chemical Wiring and Soldering toward All-Molecule Electronic Circuitry. *J. Am. Chem. Soc.*, 133:8227–8233, 2011.

[103] H. W. Ch. Postma. Rapid sequencing of individual dna molecules in graphene nanogaps. *Nano Lett.*, 10:420–435, 2010.

[104] G. F. Schneider, S. W. Kowalczyk, V. E. Calado, G. Pandraud, H. W. Zandbergen, L. M. K. Vandersypen, and C. Dekker. DNA Translocation through Graphene Nanopores. *Nano Lett.*, 10:3163–3167, 2010.

[105] C. A. Merchant, K. Healy, M. Wanunu, V. Ray, N. Peterman, J. Bartel, M. D. Fischbein, K. Venta, Z. Luo, A. T. C. Johnson, and M. Drndić. DNA Translocation through Graphene Nanopores. *Nano Letters*, 10:2915–2921, 2010.

[106] S. Garaj, W. Hubbard, A. Reina, J. Kong, D. Branton, and J. A. Golovchenko. Graphene as a Subnanometre Trans-Electrode Membrane. *Nature*, pages 190–193, 2010.

Acta Universitatis Upsaliensis

Digital Comprehensive Summaries of Uppsala Dissertations from the Faculty of Science and Technology 875

Editor: The Dean of the Faculty of Science and Technology

A doctoral dissertation from the Faculty of Science and Technology, Uppsala University, is usually a summary of a number of papers. A few copies of the complete dissertation are kept at major Swedish research libraries, while the summary alone is distributed internationally through the series Digital Comprehensive Summaries of Uppsala Dissertations from the Faculty of Science and Technology.

Distribution: publications.uu.se
urn:nbn:se:uu:diva-160474

ACTA
UNIVERSITATIS
UPSALIENSIS
UPPSALA
2011